ELEMENTA
Science of the Anthropocene

Castro de la Guardia, L, et al. 2023. Increasing depth distribution of Arctic kelp with increasing number of open water days with light. *Elem Sci Anth*, 11: 1. DOI: https://doi.org/10.1525/elementa.2022.00051

RESEARCH ARTICLE

Increasing depth distribution of Arctic kelp with increasing number of open water days with light

Laura Castro de la Guardia[1,*], Karen Filbee-Dexter[2,3,4], Jillian Reimer[1], Kathleen A. MacGregor[3,5], Ignacio Garrido[3,6,7], Rakesh K. Singh[8], Simon Bélanger[8], Brenda Konar[9], Katrin Iken[9], Ladd E. Johnson[3], Philippe Archambault[3], Mikael K. Sejr[10], Janne E. Søreide[11], and C. J. Mundy[1]

Kelps are a dominant macrophyte group and primary producer in Arctic nearshore waters that provide significant services to the coastal ecosystem. The quantification of these services in the Arctic is constrained, however, by limited estimates of kelp depth extent, which creates uncertainties in the area covered by kelp. Here, we test the environmental drivers of the depth extent of Arctic kelp. We used Southampton Island (SI), Nunavut, Canada, as an example region after an initial survey found deep Arctic kelp (at depths to at least 50 m) with relatively low grazing pressure within diverse hydrographic conditions. We found abundant rocky substrata, but no influence of substratum type on kelp cover. The kelp cover increased with depth until 20 m and then decreased (the median maximum depth for all stations was 37 m). The best predictor of kelp depth extent was the number of annual open (ice-free) water days with light ($r^2 = 44$–52%); combining depth extent data from SI with published data from Greenland strengthened this relationship ($r^2 = 58$–71%). Using these relationships we estimated the maximum kelp-covered area around SI to be $27{,}000$–$28{,}000\ \mathrm{km}^2$, yielding potential primary production between 0.6 and $1.9\ \mathrm{Tg\ C\,yr}^{-1}$. Water transparency was a key determinant of the underwater light environment and was essential for explaining cross-regional differences in kelp depth extent in SI and Greenland. Around SI the minimum underwater light required by kelp was $49\ \mathrm{mol\ photons\ m}^{-2}\ \mathrm{yr}^{-1}$, or 1.4% of annual integrated incident irradiance. Future consideration of seasonal variation in water transparency can improve these underwater light estimations, while future research seeking to understand the kelp depth extent relationship with nutrients and ocean dynamics can further advance estimates of their vertical distribution. Improving our understanding of the drivers of kelp depth extent can reduce uncertainties around the role of kelp in Arctic marine ecosystems.

Keywords: Kelp, Arctic coastal regions, Minimum light, Water transparency, Depth extent, Open water days

1. Introduction

Kelps are brown macroalgae from the order Laminariales that can form dense underwater forests in temperate and polar oceans (e.g., Dayton, 1985; Lüning, 1991; Steneck et al., 2012; Smale et al., 2013; Krause-Jensen and Duarte, 2016; Filbee-Dexter et al., 2019; Wernberg et al., 2019; Mora-Soto et al., 2021). Kelp ecosystems offer multiple benefits to the coastal region that can substantially increase local marine biodiversity (Teagle et al., 2017; Wernberg et al., 2019). Kelps are important ecosystem

[1] Centre of Earth Observation Science, University of Manitoba, Winnipeg, MB, Canada
[2] Benthic Communities Group/Institute of Marine Research, His, Norway
[3] ArcticNet, Québec-Océan, Takuvik, Département de biologie, Université Laval, Québec, QC, Canada
[4] School of Biological Science and Indian Oceans Marine Research Centre, University of Western Australia, Perth, Western Australia, Australia
[5] Demersal and Benthic Sciences Division, Maurice-Lamontagne Institute, Fisheries and Oceans Canada, QC, Canada
[6] Laboratorio Costero de Recursos Acuáticos de Calfuco (LCRAC), Instituto de Ciencias Marinas y Limnológicas (ICML), Facultad de Ciencias, Universidad Austral de Chile, Valdivia, Chile
[7] Centro FONDAP de Investigación Dinámica de Ecosistemas Marinos de Altas Latitudes (IDEAL), Universidad Austral de Chile, Valdivia, Chile
[8] Département de biologie, chimie et géographie, Université du Québec à Rimouski, Groupes BORÉAS et Québec-Océan, Rimouski, QC, Canada
[9] College of Fisheries and Ocean Sciences, University of Alaska Fairbanks, AK, USA
[10] Department of EcoScience, Arctic Research Centre, Aarhus University, Aarhus, Denmark
[11] The University Centre in Svalbard, Longyearbyen, Svalbard
* Corresponding author:
Email: laura.delaguardia@gmail.com

engineers; for example, they can modify seawater chemistry (i.e., reduce acidification), forming microenvironments that offer sanctuary to a number of canopy-dwelling species, including calcifying organisms (Krause-Jensen et al., 2016; Pfister et al., 2019; Ling et al., 2020; Murie and Bourdeau, 2020). They also have an important role in nutrient cycling (Pfister et al., 2019; Murie and Bourdeau, 2020) and can be significant carbon sinks in coastal waters (Dunton et al., 2013; Krause-Jensen and Duarte, 2016; Murie and Bourdeau, 2020; Fieler et al., 2021). Erosion, fragmentation, and dislodgement of kelp can result in carbon exports averaging 82% of annual kelp productivity in temperate regions (Krumhansl and Scheibling, 2012). Additionally, some canopy-forming kelp species can reduce coastal erosion by dissipating and absorbing 50 to 80% of the wave energy (Mork, 1996; Morris et al., 2020).

Kelps are distributed as a function of substrata, nutrients, grazing pressure, temperature, and the underwater light environment (e.g., Mohr et al., 1957; Lüning, 1991; Wiencke and Amsler, 2012; Krause-Jensen et al., 2020; Goldsmit et al., 2021; Filbee-Dexter et al., 2022). Among these drivers, the underwater light environment is probably the most significant variable influencing kelp growth in sea-ice-associated waters (Chapman and Lindley, 1980; Dunton, 1990; Bonsell and Dunton, 2018; Filbee-Dexter et al., 2019; Mora-Soto et al., 2021). The underwater light environment in the Arctic is dependent on sea ice, the insolation cycle, snow cover, and water transparency (Gattuso et al., 2006; Gattuso et al., 2020; Laliberté et al., 2021; Singh et al., 2022).

The recent loss of Arctic sea ice associated with climate change (Kern et al., 2019) has the potential to increase the amount of light reaching the seafloor (Gattuso et al., 2020). At the same time, sea ice loss in coastal waters has been linked with increased coastal erosion, riverine input, and decreased water transparency to an extent that cancels the potential increase or even decreases the underwater light availability (Bartsch et al., 2016; Bonsell and Dunton, 2018; Singh et al., 2022). Therefore, the loss of sea ice is likely to drive a change in the spatial distribution and depth extent of Arctic kelp (Hop et al., 2016; Goldsmit et al., 2021). Sea-ice-associated coastal waters that experience a decrease in underwater light, but also a lessening in ice scouring in shallow waters, could see a shift in kelp depth distribution towards shallower waters (Bartsch et al., 2016; Wiktor et al., 2022). Meanwhile, sea-ice-associated waters that experience an increase in underwater light could see a deepening of the kelp forest (Krause-Jensen et al., 2012; Hop et al., 2016; Filbee-Dexter et al., 2019; Krause-Jensen et al., 2020). Either scenario could lead to a possible increase in the overall extent of kelps in the Arctic, especially considering that Arctic kelps are well adapted to long periods in the dark and low underwater light levels, with some kelps having a compensation irradiance as low as 0.1–0.3 mol photons m^{-2} d^{-1} (Chapman and Lindley, 1980; Dunton and Jodwalis, 1988; Henley and Dunton, 1997; Borum et al., 2002).

The lower depth extent of kelps in historical records of the Eastern Canadian Arctic and sub-Arctic does not commonly exceed a depth of 25 m (Chapman and Lindley, 1980; Keats et al., 1989; Sharp et al., 2008), with most kelps in the northern hemisphere having a lower depth extent between 9 and 32 m (citing the 10 to 90% percentile (Krause-Jensen et al., 2019)). The two deepest records of kelp in the Arctic are in the Northwest Passage in the Canadian Arctic at 40 m (Bluhm et al., 2022) and in offshore Disko Bay, Greenland, 61 m (Krause-Jensen et al., 2019). Furthermore, the lower depth extent of kelps along western Greenland follows the latitudinal gradient and deepened 10–15 m at the southernmost station, where there is a high number of open water days with light (OWL, a proxy for the underwater light environment) and relatively warm waters (Krause-Jensen et al., 2012). However, when controlling for the latitudinal gradient and OWL, other environmental characteristics, such as water transparency, can become important predictors of kelp depth extent. Specifically, sites with clearer waters have deeper kelps in Arctic, temperate and tropical regions (Spalding et al., 2003; Graham et al., 2007; Krause-Jensen et al., 2019).

In northern Hudson Bay, Nunavut, Canada, a recent survey documented the abundance of kelp around Southampton Island (SI) (Filbee-Dexter et al., 2022). This survey presented a unique opportunity to investigate drivers of kelp depth extent in a physically diverse region with highly variable sea ice cover and without a strong influence of latitudinal gradient or grazing pressure. By identifying the drivers of the depth extent of Arctic kelp in this region, we aim to help improve the prediction of the total kelp forest area. This prediction is essential to improve estimates of the contribution of kelp to blue carbon and benthic primary production (Dunton et al., 2013; Krause-Jensen and Duarte, 2016; Filbee-Dexter et al., 2022). Furthermore, we combined our data on kelp depth extent with existing data from Greenland (Krause-Jensen et al., 2012; Krause-Jensen et al., 2019) to re-assess the relationship between kelp depth extent and OWL across a larger spatial scale. We hypothesized that kelp would extend to greater depths in regions with longer OWL and high water transparency.

2. Materials and methods

2.1. Study area: General description

Southampton Island is located in northwest Hudson Bay within Nunavut, Canada, between latitudes 62 and 67°N, and longitudes 88 and 80°W. The island covers approximately 52,000 km^2 and has 1,400 km of coastline. The surveys were conducted during the periods of 10–22 August 2018 and 4–29 August 2019 primarily around SI, but also included the neighbouring Coats Island and the nearby mainland (**Figure 1**). Twenty-one locations, separated by an average distance of 67 km (range: 10–175 km), were selected to sample transects perpendicular to the coast (i.e., along the depth gradient), hereafter referred to as stations. The latitude and longitude for a station was defined as the average of the positions of all sampling locations along the transect (Table S1). The goal was to provide maximum coverage around the island (**Figure 1**). However, due to inclement weather conditions in August

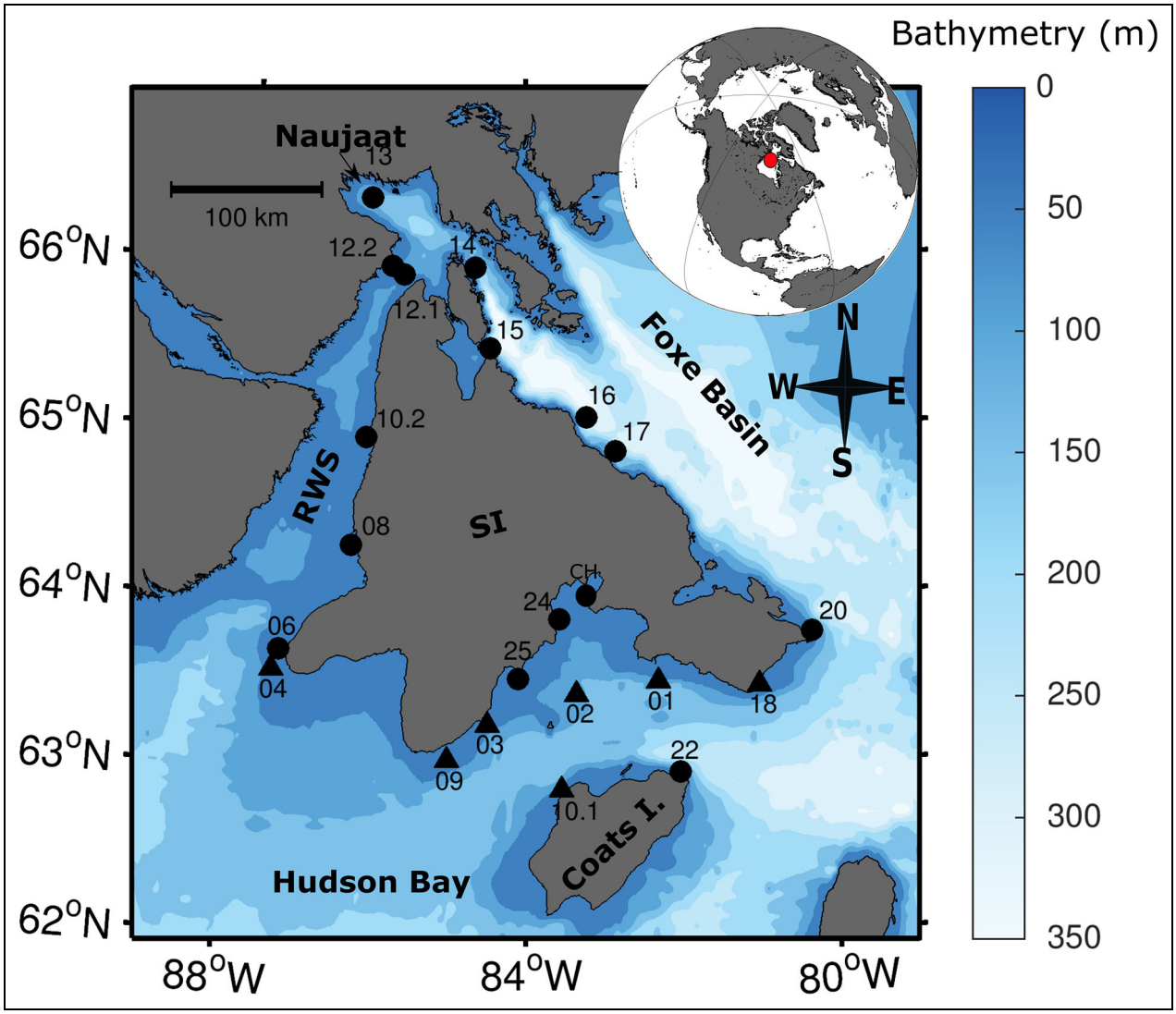

Figure 1. Regional bathymetry of the study area and survey stations in 2018 (triangles) and 2019 (circles). Inset map on the top right shows the location of study area (red dot) in northern Hudson Bay. Survey stations were located along the coasts of Southampton Island (SI), Coats Island (Coats I.) and Roes Welcome Sound (RWS). Bathymetry data (color–scale bar) were derived from global relief gridded data ETOP1 (Amante and Eakins, 2009; NOAA, 2009).

2018, only the southern side of the island was visited, and three stations (01, 10.1 and CH) were not sampled adequately to be included in the analyses (i.e., maximum sampled depth was shallower than 20 m or fewer than three depths were surveyed along a transect).

2.2. Kelp cover, depth extent, and substrata

Kelp cover was estimated using a drop-camera (Black 7 GoPro) secured to a GroupBinc wing attachment and a 2.3 kg weight following the method of Filbee-Dexter and Scheibling (2017). Sampling took place from either a rigid-hull inflatable boat or the main vessel, the R/V *William Kennedy*. At each station, the drop-camera was lowered to the seafloor at 5-m depth intervals, starting from the 5-m isobath and ending with the 50-m isobath. The minimum and maximum target depths were set by logistical constraints: sampling in waters shallower than 5 m was prevented due to the main vessel's draft, and sampling in waters deeper than 50 m was prevented by the camera housing pressure limitation. The relatively small semidiurnal tidal range in the region of approximately 1–2 m (Prinsenberg and Freeman, 1986; Saucier et al., 2004; Luneva et al., 2015; Tideschart, 2022) allowed us to use uncorrected depth measurements for this study.

The drop-camera was lowered to the bottom and then held between 1 and 2 m above the seafloor, recording a video for 1–3 min while drifting with the boat or vessel. Still frames were randomly extracted from the videos, and a single frame was selected based on best observed image quality. The field of view of the camera (frame size) was at least 1 m^2. The full image was analyzed to determine kelp percent cover, dominant kelp assemblage (high-canopy or low-canopy), and substratum type (rocky, sandy or mixed). The percentage kelp cover was estimated as a function of the percentage of the image covered by kelp (0–100%), thus the exact size of the image was not critical. To

estimate the percentage kelp cover we used a combination of the software ImageJ (Schindelin et al., 2012) and visual verification, which helped to avoid the inclusion of detached kelps and non-kelp species of algae. Canopy height classification of high-canopy reflected the dominance of large adult high-canopy-forming kelp species extending vertically off the seafloor (specifically, *Saccharina latissima* with hollow buoyant stipes and mixed *Alaria esculenta* and *Laminaria solidungula*); low-canopy classification was used when there was no visible upright stipe (typically *Agarum clathratum* and sparse, small stands of low-lying kelp juveniles or small adults). Rocky substratum was composed of mostly rocks and/or pebbles, whereas sandy substratum included mostly sand. Mixed substratum was composed of sand, rocks and pebbles in different proportions. We assumed that the observable substratum in any given image frame was representative of the entire image, even on images where less than 10% of the seafloor was visible due to high kelp cover. This assumption is consistent with diver observations of the substrata under the canopy at nearby sites (Filbee-Dexter et al., 2022). Example images of these classifications can be seen in Figure S1).

The depth extent of kelp at each station (Table S2) was defined for the deepest occurrence of each of the four targeted percentage kelp covers (i.e., 80, 50, 10 and 1% kelp cover), following Krause-Jensen et al. (2012) but using linear interpolation between neighbouring 5-m depth intervals to reach the exact percentage cover. When the maximum percentage kelp cover at a station was smaller than the targeted percentage, or when the percentage kelp cover at the deepest survey depth was larger than the targeted percentage, we were not able to identify the depth extent associated with the targeted percentage kelp cover. These stations were subsequently excluded from the depth extent analysis for the target percentage kelp cover. Table S2 lists the stations that were included in the depth extent analysis for each percentage kelp cover (N = 11, 13, 12 and 9 stations for the 1, 10, 50 and 80% kelp cover, respectively).

2.3. Characterization of the coastal environment

August upper water column temperature and salinity data were taken from the World Ocean Atlas database (WOA18) (Locarnini et al., 2018; Zweng et al., 2018). The most recent climatology period (2005–2017) available on the site was selected and used to describe the average regional conditions. In situ vertical profiles of temperature, salinity, photosynthetically available radiation (PAR), and chlorophyll-a fluorescence were measured using a conductivity, temperature, and depth profiler (CTD, Seabird 19plus) with Biospherical scalar PAR and Seabird ECOtriplet fluorometer sensors (Mundy, 2017). These profiles were taken in August 2018 and 2019 at the same time as the kelp cover estimates. The CTD was lowered using the ship's winch. Usually, only one CTD profile was taken per station, but when more than one CTD profile was available, we selected the deepest profile with the least amount of noise. From these profiles we extracted the averaged upper water column temperature ($T_{0-30\mathrm{m}}$) and salinity ($S_{0-30\mathrm{m}}$). We defined the euphotic depth (Z_{eu}) as in Ryther (1956) and calculated the downwelling diffused light attenuation coefficient for PAR (κ_{dPAR}) within the euphotic zone using the method of Weiskerger et al. (2018) with modifications described in the following subsection. We also estimated water stratification as the maximum value of the Brunt-Väisälä frequency (N^2) within the upper water column, the depth of the chlorophyll-a maximum (Z_{chl}), and the depth-integrated chlorophyll-a concentration ($iChl$) within the euphotic zone or top 30 m when Z_{eu} was greater than the water depth. Additionally, for the depth extent analysis, we also obtained the CTD temperature and salinity at the depth extent of 80, 50, 10 and 1% kelp cover (T_z and S_z; Table S2). We defined the upper water column in the depth range of 1.5–30 m, based on the median depth (29 m) at which kelps were observed around SI; the upper limit (1.5 m) was chosen to ensure a full submersion of the sensors.

2.4. Calculating Z_{eu} and κ_{dPAR} from the vertical profile of PAR

We followed the iterative method of Weiskerger et al. (2018) to estimate κ_{dPAR} and Z_{eu} from the vertical profiles of PAR. First, we estimated PAR just below the ocean surface, PAR^{0-} using the upper part of the PAR profile (depth: 1.5 to 10 m). PAR^{0-} was estimated as the intercept of the linear least-squares-regression fitting of the natural logarithm (ln) transformed PAR versus depth, z. Second, we standardized the PAR profile as follows: standard $PAR_z = 100 \times PAR_z/PAR^{0-}$. Third, we estimated Z_{eu} using the standardized PAR profile as the depth closest to standard $PAR_z = 1\%$ (Ryther, 1956). Finally, PAR_z values beyond the Z_{eu} were removed, and κ_{dPAR} was estimated using the Beer-Lambert Law ($ln(PAR_z) = ln(PAR^{0-}) - \kappa_{dPAR} \times z$). This methodology creates a dependency of κ_{dPAR} on the euphotic depth, thus resulting in a negative correlation between Z_{eu} and κ_{dPAR} (Spearman Rank correlation: $r = -0.99$, $p < 0.05$).

2.5. Defining open water days with light (OWL)

OWL was defined following Krause-Jensen et al. (2012) as the number of ice-free days with daylight, whereby ice-free days were defined as days with sea ice concentration below 15%, and days with daylight were defined as days outside of the astronomical dark period. Here, we adjusted the definition of "days with daylight" to "days with surface PAR greater than 10 mol photons m^{-2} d^{-1}." This threshold was chosen because it leads to a first-order estimation of transmitted PAR of 0.21 mol photons m^{-2} d^{-1} at 29 m, the median depth at which kelps were observed around SI. The value of 0.21 mol photons m^{-2} d^{-1} approximates the mean compensation irradiance for *Laminaria solidungula* and *Saccharina latissima*, two of the most common kelp species in the region (Filbee-Dexter et al., 2022). For *L. solidungula* the estimated compensation irradiance ranges between 0.13 and 0.26 mol photons m^{-2} d^{-1} (Chapman and Lindley, 1980; Dunton and Jodwalis, 1988; Henley and Dunton, 1997), and for *S. latissima* it ranges between 0.17 and 0.4 mol photons m^{-2} d^{-1} (King and Schramm, 1976; Borum et al., 2002).

Ice-free days were selected using a 10-day running mean of daily ice concentration to smooth out data noise (Krause-Jensen et al., 2012). For stations around SI, we used 2017–2019 sea-ice data derived using the Advanced Microwave Scanning Radiometer 2 (AMSR2) on the NASA Aqua Satellite with a daily temporal resolution and 6.25 km^2 spatial resolution (Spreen et al., 2008). For stations around Greenland, we used sea-ice data from 2007–2009, which corresponded to the timing of the survey there (Krause-Jensen et al., 2012; Krause-Jensen et al., 2019). Data were derived from bootstrap version 3 algorithm (Comiso, 2017) with daily temporal resolution and 25-km^2 spatial resolution (as the higher resolution AMSR2 data are not available before 2012). Both sea ice concentration datasets have a negative bias of about 20% during the period of low sea ice concentration relative to ship-based observations (Spreen et al., 2008; Kern et al., 2019), implying a potential overestimation in the number of ice-free days around Greenland and SI.

2.6. Estimating surface and underwater PAR from a shortwave radiation model

We estimated daily PAR (mol photons m^{-2} d^{-1}) just above the ocean or sea ice surface (PAR^{0+}) from the integration of hourly (h) total shortwave radiation (SW in W m^{-2}) in the 400–700 nm spectral band (Equation 1). Hourly SW radiation was obtained from the Canadian Meteorological Centers Global Deterministic Prediction System with a 25 km^2 spatial resolution (Smith et al., 2014). This atmospheric reanalysis forecast model includes cloud cover.

$$PAR^{0+} = \sum_{h} SW \times 0.46 \times 4.57 \times 3600 \quad (1)$$

In this equation, PAR^{0+} is parameterized as $SW \times 0.46$ (Kvifte et al., 1983). The units are then converted from W m^{-2} to μ mol photons m^{-2} s^{-1} by multiplying by a conversion factor of 4.57 (Sager and McFarlane, 1997) and then converting from seconds to hours by multiplying by $3,600$ s. Hourly values were then integrated over one day. A 10-day running mean was applied to the daily PAR data before selecting days with light ($PAR^{0+} > 10$ mol photons m^{-2} d^{-1}). We then estimated annual surface light, $iPAR^{0+}$, which is defined as the OWL-integrated PAR^{0+}.

We estimated annual underwater light at the kelp depth extent ($iPAR_z$) at all stations using $iPAR^{0+}$ and measured κ_{dPAR}. We first parameterized the light just below the ocean surface $iPAR^{0-}$ from $iPAR^{0+}$ assuming a mean loss of light at the air-sea interface of 8%: $iPAR^{0-} = 0.92 \times iPAR^{0+}$ (Bélanger et al., 2013). The 8% represents the average loss of light (range of 6 to 10%) by scattering and reflection as it crosses the air-ocean interface at high latitudes (Morel, 1991). We then used the Beer-Lambert Law, but replaced PAR^{0+} by PAR^{0-} following the work of Bélanger et al. (2013) and Singh et al. (2022). We did not have the data to account for seasonal changes in water transparency; thus, κ_{dPAR} was assumed to be constant. Seasonal changes in water transparency, however, may result from phytoplankton blooms or increases in turbidity due to runoff and/or storm-driven resuspension (Lund-Hansen et al., 1997; Aumack et al., 2007; Hop et al., 2016; Bonsell and Dunton, 2018), with runoff being very small around SI.

2.7. Kelp depth extent data from western Greenland and offshore Disko Bay

Kelp depth extent data from western Greenland and offshore Disko Bay were obtained from published work (Krause-Jensen et al., 2012; Krause-Jensen et al., 2019). The western Greenland data were derived from eight stations across a large latitudinal range, from Nuuk at 64.1°N to Siorapaluk at 78.0°N (Table S3). Offshore Disko Bay data were obtained from four stations of similar latitudes (Rifkol at 68.0°N, Kronprinsens Ejland at 69.0°N, Hunde Ejland at 68.9°N and Hareøen at 70.4°N), and these stations had three depth transects each (Table S3). Disko Bay depth extent data were only available for 1% kelp cover. Similar to the present study, kelp depth extent data along western Greenland and Disko Bay were acquired using video transects running perpendicular to the shore and extending from nearshore to the deepest occurrence of standing kelp (Krause-Jensen et al., 2012; Krause-Jensen et al., 2019). The kelp species observed in western Greenland and Disko Bay were similar to those around SI. For the depth extent analysis, we averaged offshore Disko Bay data across station-based transects to have one value per station. The geographic locations of the stations were used to recalculate the OWL and estimate $iPAR^{0+}$, which were then used along with κ_{dPAR} to estimate $iPAR_z$. We did not estimate $iPAR_z$ at stations where κ_{dPAR} was not available.

2.8. Statistical analysis

All analyses were performed in Matlab vR2020b using numerical resources from Compute Canada on the Graham supercomputer. Normality of the data was assessed with the Kolmogorov-Smirnov test. We used a non-parametric test, Kruskal-Wallis H test (H-test), to assess differences between group medians. The H-test is reported using the level of significance (p) and Chi-squared (χ^2) value with the groups and error degrees of freedom (df) separated by a comma as subscripts (i.e., $\chi^2_{df1,df2}$).

We used the Spearman Rank partial correlation to determine the degree of association between variables considered (T, S, Z_{chl}, N^2, $iChl$, OWL, κ_{dPAR}). Only variables that were not significantly correlated were included in the stepwise multiple linear regression analysis, which was used to identify the most important variable(s) driving the kelp depth extent around SI. The stepwise model iteratively includes or excludes predictors based on the model's adjusted r^2 improving by at least 0.1 while maintaining a model significance of $p \leq 0.05$. Best models are significant ($p \leq 0.05$) and have high values of adjusted r^2.

We used a general linear F-test to evaluate if the kelp depth extent versus OWL relationships were similar in different regions. We report the linear F-test results with the F-statistic (F^*), and its F-critical value ($F^c_{df1,df2,p}$) with degrees of freedom and p shown as subscript. A similar relationship among regions (i.e., non-significant F-test) would allow us to combine all the multi-regional data for a more robust kelp depth extent versus OWL relationship. We measured the predictive potential of OWL on the kelp

depth extent data using a least-squared linear regression and report the regression results with the r^2, level of significance (p), and the equation. Outliers were defined using the interquartile range, and excluded from the analysis.

Some of the analysis required using data from the gridded products at each station (i.e., sea ice, PAR, WOA18, and OWL). We used the value from the nearest grid cell to the location of the station. When the resolution of the gridded product was too coarse, such that a station was located on a grid cell containing land, the nearest water point was selected instead.

3. Results

3.1. Southampton Island hydrography and OWL days

August T_{0-30m} and S_{0-30m} climatology maps show the relative diversity of the coastal environments around SI (**Figure 2a** and **b**). In terms of the temperature distribution (**Figure 2a**), we identified two coastal regions, a cold region along the northeast coast facing Foxe Basin ($T \leq 0°C$) and a relatively warmer region along Roes Welcome Sound and the southern coast ($T \geq 3°C$). In terms of the salinity distribution (**Figure 2b**), we identified three coastal regions, a low salinity region along the southeast coast facing Coats Island ($S \leq 31$), a high salinity ($S > 32$) region along the northwest coast within Roes Welcome Sound, and a region with mixed salinity signature lying between the high and low salinity coastal regions to the northeast and southwest of SI. The spatial variability in the length of OWL generally followed the sea surface temperature pattern (**Figure 2c**), with the shortest OWL (<100 d yr^{-1}) along the northeast coast where the sea temperature was lower. However, pockets of long OWL (>120 d yr^{-1}) were found in polynya regions along the northwest and southern coasts.

Median temperature (T_{0-30m}) and salinity (S_{0-30m}) sampled in situ was 2.7°C (mean ± standard error (SE) = 2.8 ± 0.4°C, $N = 21$) and 31.5 (31.2 ± 0.2, $N = 21$), respectively. These measured values did not differ significantly from the station climatology T_{0-30m} (H-test $\chi^2_{1,40} = 0.2$; $p = 0.7$) and S_{0-30m} ($\chi^2_{1,40} = 1.2$; $p = 0.3$), allowing us to conclude that measurements in 2018 and 2019 were representative of an average year. Co-variability between OWL, in situ T_{0-30m} and S_{0-30m}, and additional variables measured during our sampling (N^2, κ_{dPAR}, Z_{chl}, $iChl$) was tested using a Spearman rank correlation (Table S4). We found co-variability between $iChl$ and three variables, T_{0-30m} ($r = -0.62$; $p = 0.03$), κ_{dPAR} ($r = -0.64$; $p = 0.02$), and OWL ($r = -0.68$; $p = 0.02$), and between Z_{chl} and OWL ($r = -0.60$; $p = 0.04$).

3.2. Kelp ecosystem characteristics

Kelps around SI extended over the full range of depths sampled (5–50 m). The percentage kelp cover was highly variable between 5 and 30 m, but in general it increased with depth up to approximately 30 m and then decreased (Figure S2). Sea urchins and other prominent grazers, which could influence kelp depth distribution independently of the physical environment, were uncommon at all stations. The green sea urchins (*Strongylocentrotus droebachiensis*), a main grazer of kelp in the North Atlantic, were observed in drop camera images in 2018 at one station close to Coral Harbour, Nunavut (red star in **Figure 2a**). The drop camera captured one green sea urchin at 10 m and over 20 green sea urchins at 20 m. This station, however, was excluded from our analyses due to the low image quality and low visibility below 20 m. The green sea urchins were not observed in images or by divers in 2019 (Filbee-Dexter et al., 2022).

The kelp assemblages were composed primarily of perennial species, with the high canopy dominated by *Saccharina latissima*, *Alaria esculenta*, *Laminaria solidungula* and the low canopy dominated by *Agarum clathratum* and kelp juveniles or small adults. The kelp *S. latissima* extended highest into the water column due to its hollow, buoyant stipe (average stipe length of 1.5 m K. Filbee-Dexter, unpublished data), and often formed mixed stands with *A. esculenta* and *L. solidungula* (Filbee-Dexter et al., 2022). Sampling depths where the high-canopy kelp dominated had higher percentage kelp cover (median = 73%) than depths where the low-canopy kelp dominated (median =39%; H-test $\chi^2_{1,71} = 14.6$; $p < 0.05$; **Figure 3a**). The median depth of images where the dominant kelp assemblage was high-canopy was shallower than the median depth of images where the dominant kelp assemblage was low-canopy (although marginally not significant; H-test $\chi^2_{1,70} = 3.5$; $p = 0.058$). High-canopy kelps were not observed in images taken in waters deeper than 38 m while the maximum depth of images with only low-canopy kelps extended to almost 50 m (**Figure 3b**).

Rocky substrata were more abundant than sandy and mixed substrata. From the total of 117 drop-camera images, 71 had rocky substrata, 20 had sandy substrata, 19 had mixed substrata, and 7 images had undetermined substrata because high kelp cover masked the seafloor. The substratum type did not influence the percentage of kelp cover (H-test $\chi^2_{2,64} = 0.7$; $p = 0.7$; **Figure 3c**), but it did influence kelp canopy height (H-test $\chi^2_{2,62} = 8.4$; $p = 0.01$). Specifically, mixed substrata were more likely to host low-canopy kelps relative to rocky (H-test $\chi^2_{1,54} = 8.2$; $p < 0.05$) and sandy (H-test $\chi^2_{1,15} = 4.8$; $p = 0.03$) substrata. Mixed substrata were also observed in significantly deeper waters (median depth = 32 m) relative to rocky (median depth = 24 m; H-test $\chi^2_{1,88} = 6.6$; $p = 0.01$) and sandy (median depth = 22 m; H-test $\chi^2_{1,37} = 6.3$, $p = 0.01$) substrata (**Figure 3d**).

A similar analysis as the one presented in **Figure 3** was performed considering only images at the depth extent of each targeted percentage of kelp cover (i.e., 80, 50, 10 and 1%) at each station. This analysis revealed no significant difference in regards to canopy height or substratum type at the depth extent (Figure S3). However, at the depth extent of the 80% kelp cover the number of stations with high-canopy kelps ($N = 6$) outnumbered stations with low-canopy kelps ($N = 2$; Figure S3g), and stations with rocky substrata ($N = 7$) outnumbered stations with sandy substrata ($N = 1$; Figure S3h).

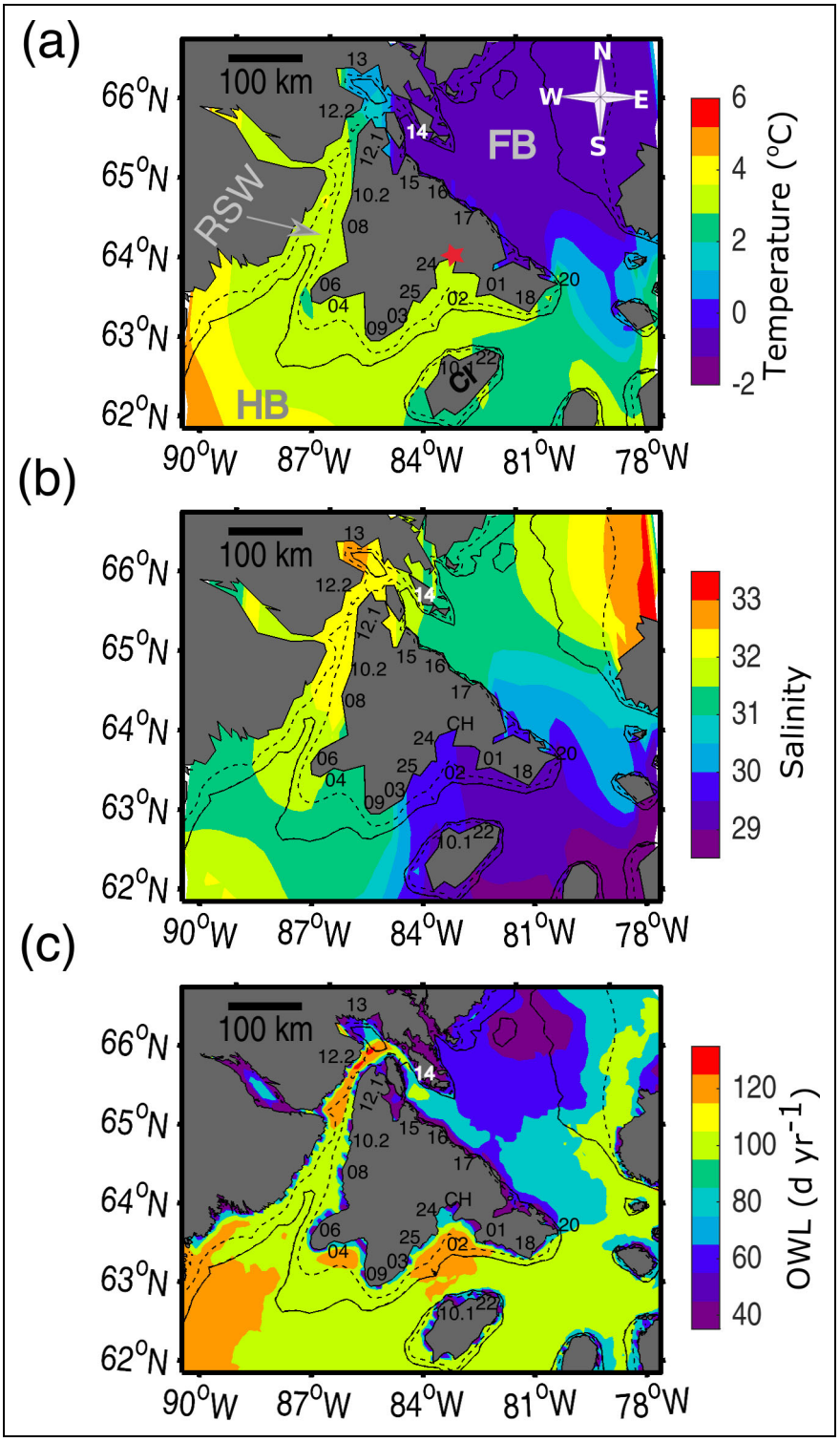

Figure 2. Hydrographic variation around Southampton Island. August climatology (2005–2017) of (a) surface temperature (T_{0-30m}) and (b) salinity (S_{0-30m}) from the World Ocean Atlas database (WOA18) (Locarnini et al., 2018; Zweng et al., 2018). (c) Averaged (2017–2019) annual number of open water days with light (OWL). Maps are overlaid with the approximate location of kelp survey stations. Contour lines are the 50-m (dashed) and 100-m (solid) isobaths. Acronyms for oceanic regions are shown in (a) Foxe Basin (FB), Hudson Bay (HB), Roes Welcome Sound (RSW) and Coats Island (CI). Red star in (a) marks the only station where sea urchins (*Strongylocentrotus droebachiensis*) were observed.

3.3. OWL as the driver of kelp depth extent

We evaluated the drivers of the depth extent of kelp using stepwise linear regression with five explanatory variables (T_z, S_z, N^2, OWL, κ_{dPAR}; Tables S1–S2). Other variables measured during our survey ($iChl$, Z_{chl}) were not included in this analysis because they correlated with either OWL or

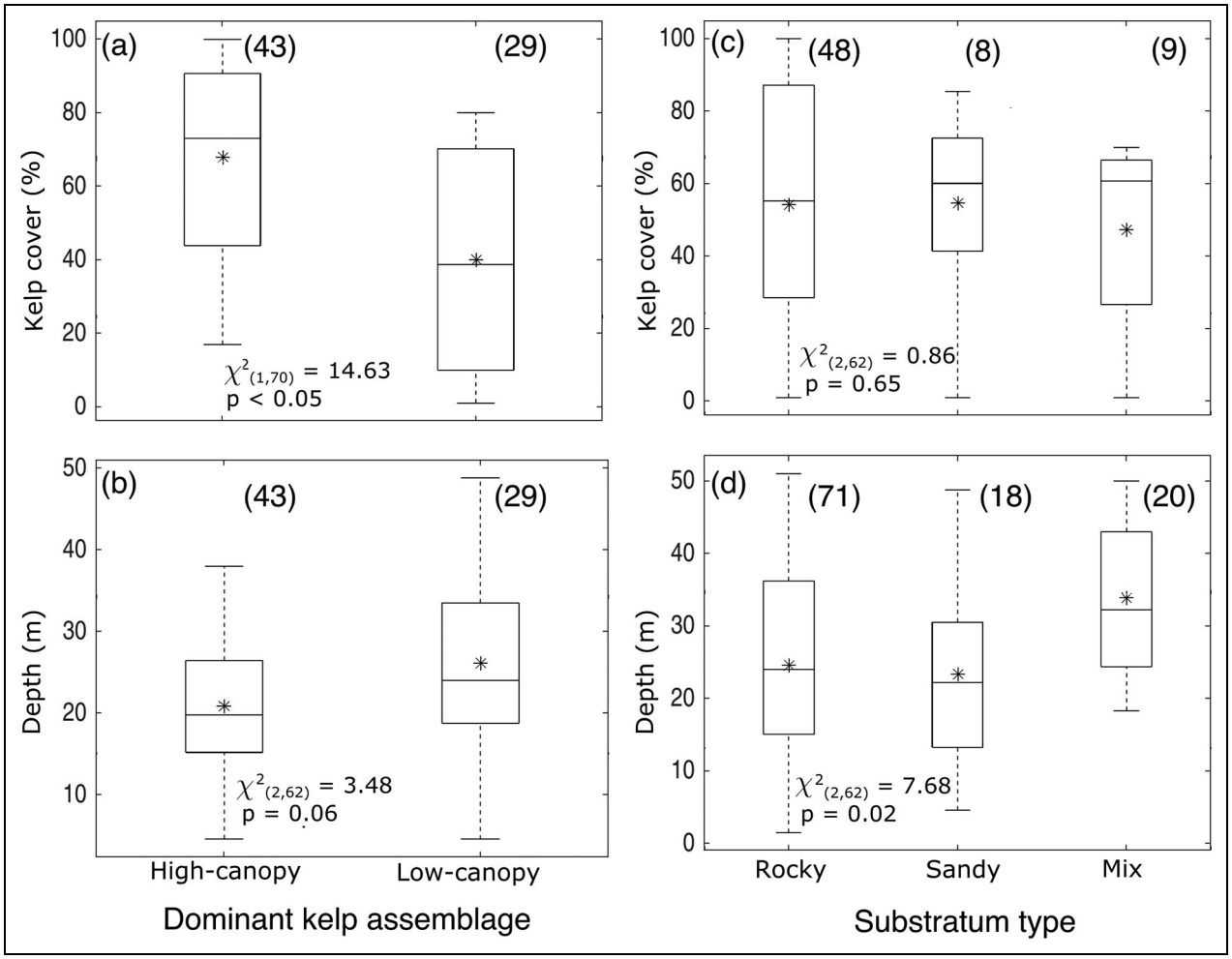

Figure 3. Percentage kelp cover and depth of kelp forests around Southampton Island. Data are grouped according to the dominant kelp assemblage (a and b) and substratum type (c and d). A non-parametric Kruskal-Wallis H-test was used to assess significant difference between groups (groups are significantly different if $p \leq 0.05$). Statistics presented in boxplot are the 25^{th} and 75^{th} percentiles as bottom and top edges of the box, respectively, the minimum and maximum as the whiskers, the median as central line, and the mean indicated by the star. The numbers in parentheses are the number of images included in each group.

Table 1. Simple linear regression models predicting kelp depth extent from open water days with light (OWL), with coefficient of determination (r^2) and level of significance (p)

Equation			r^2	p
depth extent of 1% kelp cover	=	$6.2 + 0.3\times$ OWL	0.44	0.025
depth extent of 10% kelp cover	=	$3.5 + 0.3\times$ OWL	0.50	0.007
depth extent of 50% kelp cover	=	$-5.8 + 0.4\times$ OWL	0.52	0.008
depth extent of 80% kelp cover	=	$-4.3 + 0.3\times$ OWL	0.44	0.050

κ_{dPAR} (Table S4). The four linear regression models were significant ($p \leq 0.05$) and had a relatively high adjusted $r^2 \geq 0.44$. From the five explanatory variables only OWL was selected by the stepwise regression model. Subsequently, simple linear regression was used to show that OWL explained between 44 and 52% of the variability in the kelp depth extent (**Table 1**).

For a more general assessment of the relationship of kelp depth extent and OWL over a wider spatial scale we combined our kelp depth extent data from SI with published data from western Greenland and Disko Bay (Krause-Jensen et al., 2012; Krause-Jensen et al., 2019). Most of the Greenland data followed the same general pattern of larger OWL leading to deeper kelp; however, two stations in western Greenland, Nuuk-1 and Itelleq, did not follow the same trend (circled red in **Figure 4**). These two stations had the largest OWL but a relatively shallow kelp depth extent. Using a robust linear fit, we found that the two stations had the largest residuals. Furthermore, the OWL length at Nuuk-1 and Itelleq were outliers of the combined data. For these reasons, we excluded these two stations from the general linear F-test and kelp depth extent analysis presented below.

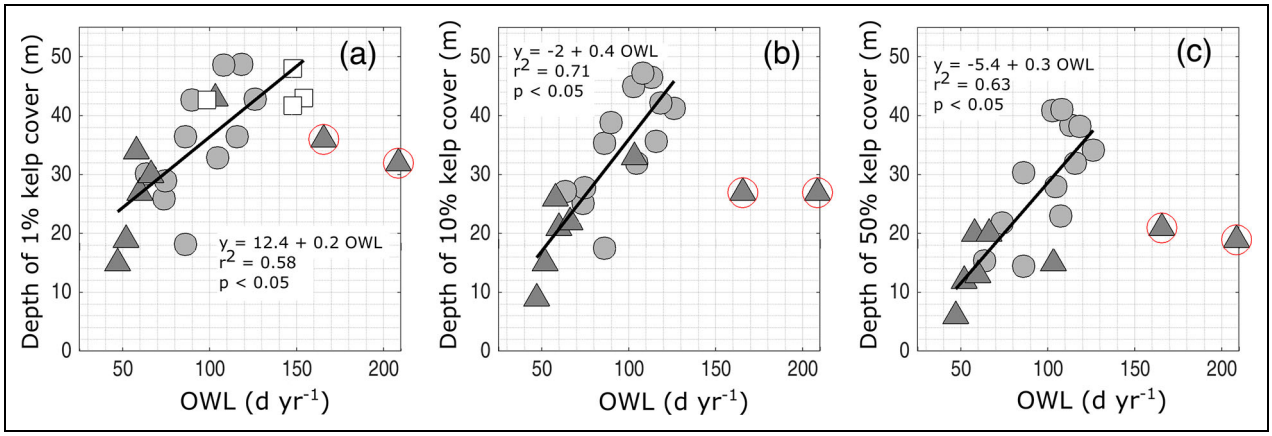

Figure 4. Kelp depth extent as a function of open water days with light (OWL). Relationships between the depth of (a) 1%, (b) 10%, and (c) 50% kelp cover and OWL for data from Southampton Island (light grey circles), western Greenland (dark grey triangles) and offshore Disko Bay (white squares). Each point represents one station; Disco Bay depth extent data are only available for the 1% kelp cover in (a). The black line in (a)–(c) is the linear regression excluding outliers (stations circled in red).

A general linear F-test analysis was performed to determine whether to accept ($F^* < F^c$; i.e., not significant) the reduced model that combines data from SI, western Greenland, and Disko Bay on a single kelp depth extent versus OWL relationship, or to reject ($F^* > F^c$, i.e., significant) the reduced model in favour of the larger model with independent relationships. The results of the general linear F-test for the relationships of 1% kelp cover depth extent versus OWL were not significant, suggesting that we can accept the reduced model ($F^* = 1.14$; $F^c_{19,15,0.05} = 2.34$) and combine Disko Bay, western Greenland, and SI datasets (**Figure 4a**). Similarly, the reduced model was accepted on the relationships of kelp depth extent versus OWL for 10% ($F^* = 0.37$; $F^c_{17,15,0.05} = 2.37$) and 50% ($F^* = 2.00$; $F_{16,14,0.05} = 2.45$) kelp covers (**Figure 4b** and **c**), implying that the regional datasets could be combined in a single relationship. Least squares linear regression between kelp depth extent and OWL for the combined dataset explained 58, 71, and 63% of the variability for the 1, 10, and 50% kelp cover depth extent, respectively (**Figure 4a–c**). These r^2 coefficients (range of 0.58–0.71) were larger than considering SI data alone (range of 0.44–0.52; **Table 1**).

Using the relationships of OWL versus depth extent presented in **Table 1**, we estimated the potential present-day kelp habitat around SI, assuming suitable substrata present (**Figure 5**). The maximum total area (with at least 1% kelp cover) was estimated at approximately 28,000 km^2, and the total area with at least 10, 50 and 80% kelp cover was estimated at approximately 27,000, 25,000 and 20,000 km^2, respectively. The same can be done using the relationship from **Figure 4**, which would yield only a slightly smaller total area estimate of approximately 27,000, 28,000 and 19,000 km^2 with at least 1, 10 and 50% kelp cover, respectively.

3.4. Cross-regional comparison of depth extent and underwater light environment

Comparing the kelp depth extent of categories of percentage kelp cover highlighted relationships of increasing percentage kelp cover with decreasing depth (linear regression: $r^2 = 0.95$; $p = 0.03$; **Figure 6a**) and increasing PAR (linear regression: $r^2 = 0.93$; $p = 0.04$; **Figure 6b**). Around SI, the median depth extent of the 80% kelp cover category was 25 m (mean ± SE = 23 ± 3 m, $N = 9$), receiving mean annual light of $iPAR_z = 234 \pm 90$ mol photons m^2 yr^{-1}, $N = 8$ (approximately 8% of $iPAR^{0+}$; Table S2). At the deep end, the median depth extent of the 1% kelp cover was 40 m (37 ± 4 m, $N = 11$), receiving a mean $iPAR_z$ of 49 ± 32 mol photons m^2 yr^{-1}, $N = 8$ (approximately 1.4% of $iPAR^{0+}$; Table S2). The latter also defines the minimum underwater light required by kelp around SI. Around SI, the 1 and 10% kelp cover did not differ in depth extent (combined mean 37 ± 2 m, $N = 24$; H-test: $\chi^2_{1,16} = 0.2$; $p = 0.7$) or $iPAR_z$ (combined mean 49 ± 20 mol photons m^2 yr^{-1}, $N = 18$; H-test: $\chi^2_{1,16} = 0.5$; $p = 0.5$); however, in the following analysis the 1 and 10% kelp cover were separated in order to compare to western Greenland and offshore Disko Bay datasets.

The depth extent of the 1% kelp cover along western Greenland coast, offshore Disko Bay and around SI was similar (H-test: $\chi^2_{2,15} = 4.72$; $p = 0.09$) with a combined mean of 36 ± 3 m, $N = 21$. The $iPAR_z$ at the maximum depth extent of the 1% kelp cover of stations along western Greenland was also similar to SI (H-test: $\chi^2_{1,11} = 0.2$; $p = 0.6$) with a combined mean of 39 ± 20 mol photons m^{-2} yr^{-1}, $N = 14$. The depth extent of the 10 and 50% kelp cover was significantly deeper around SI relative to western Greenland (H-test: $\chi^2_{1,17} = 6.8$; $p < 0.05$, for the 10%; H-test: $\chi^2_{1,16} = 6.0$; $p < 0.05$, for the 50%; **Figure 6a**). The median depth extent of the 10% kelp cover was 40 m (37 ± 3 m, $N = 13$) around SI and 22 m (21 ± 3 m, $N = 6$) along western Greenland. The median depth extent of the 50% kelp cover around SI was 36 m (32 ± 4 m, $N = 12$) and along western Greenland it was 14 m (14 ± 2 m, $N = 6$). Despite the deeper depth extent of kelp around SI, $iPAR_z$ at the depth extent of the 10 and the 50% kelp cover did not differ between the two regions (H-test: $\chi^2_{1,13} = 0.5$; $p = 0.5$, for the 10%; and H-test: $\chi^2_{1,11} = 1.1$; $p = 0.3$ for 50%). The

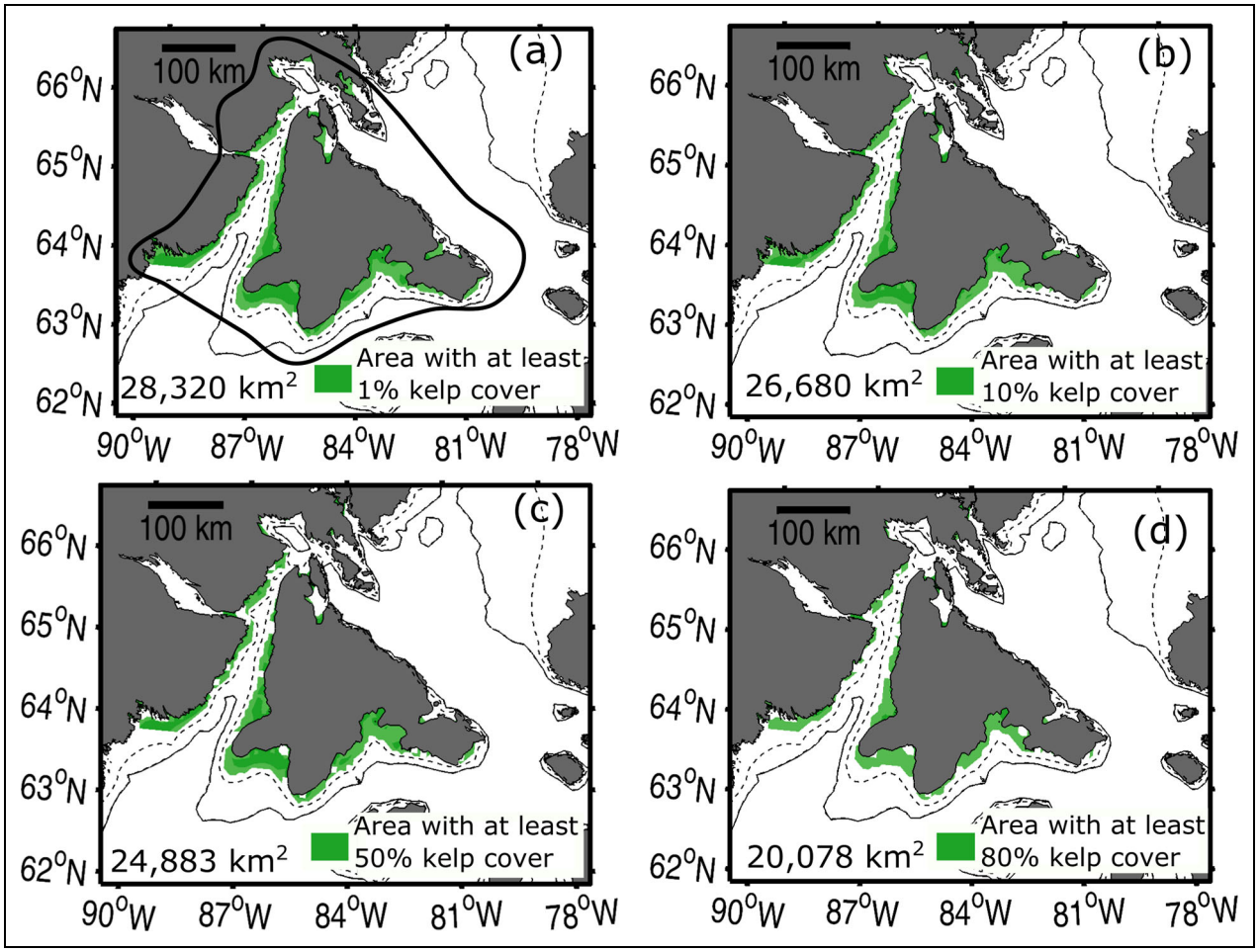

Figure 5. Estimates of present-day kelp depth extent around Southampton Island. Estimates were made using the relationships between depth extent and open water days with light (OWL) in **Table 1**. Green indicates the area estimated to have kelp forest with at least (a) 1% kelp cover, (b) 10% kelp cover, (c) 50% kelp cover and (d) 80% kelp cover. The number on the bottom left of each panel is the total area covered by kelp. Contour lines are the 50 m (dashed) and 100 m (solid) isobaths. The estimation was only done within the area encircled by the solid thick black line in (a).

mean $iPAR_z$ at the depth extent of the 10% kelp cover for the two regions combined (western Greenland and SI) was 53 ± 22 mol photons m^{-2} yr^{-1}, $N = 15$, and at the maximum depth extent of the 50% kelp cover was 124 ± 40 mol photons m^{-2} yr^{-1}, $N = 13$. The two regions also had similar length of OWL (H-test: $\chi^2_{1,30} = 1.1$; $p = 0.3$) and similar OWL-integrated surface PAR (H-test: $\chi^2_{1,30} = 2.1$; $p = 0.1$). However, water turbidity, κ_{dPAR}, was significantly lower around SI (H-test: $\chi^2_{1,17} = 6.9$; $p < 0.05$). The median κ_{dPAR} around SI was 0.13 m^{-1} (mean $\pm$ SE $= 0.13 \pm 0.01$ m^{-1}, $N = 15$) and along western Greenland it was 0.18 m^{-1} (0.17 ± 0.01 m^{-1}, $N = 5$; Krause-Jensen et al., 2012).

4. Discussion

Emerging evidence shows that Arctic kelp ecosystems can be abundant and widely distributed; however, the uncertainties in estimating the depth extent are a key constraint to quantifying their total extent and therefore estimating the ecosystem functions and benefits they provide (e.g., Hop et al., 2016; Krause-Jensen et al., 2019; Goldsmit et al., 2021; Filbee-Dexter et al., 2022). Our depth extent analysis reveals that kelps can extend beyond 40 m in some parts of SI, supporting the generality of recent studies showing kelp ecosystems extending below 30 m from Arctic to equatorial regions (Spalding et al., 2003; Graham et al., 2007; Hop et al., 2016; Krause-Jensen et al., 2019).

The kelp species composition around SI was typical of ice-covered waters in the western Arctic and Subarctic, dominated by the perennial high-canopy species *Saccharina latissima*, *Alaria esculenta*, *Laminaria solidungula*, and the low-canopy species *Agarum clathratum* (e.g., Chapman and Lindley, 1980; Dunton and Jodwalis, 1988; Borum et al., 2002; Spurkland and Iken, 2011a; Filbee-Dexter et al., 2019; Bonsell and Dunton, 2021; Filbee-Dexter et al., 2022). Kelps followed a gradient of increasing cover moving offshore to around 20 m, which is consistent with zonation patterns from other Arctic coastlines where sea ice scours the seafloor in the nearshore zone supporting little to no macroalgae (Chapman and Lindley, 1980; Borum et al., 2002; Sharp et al., 2008; Filbee-Dexter et al., 2022). Furthermore, landfast ice cover has been

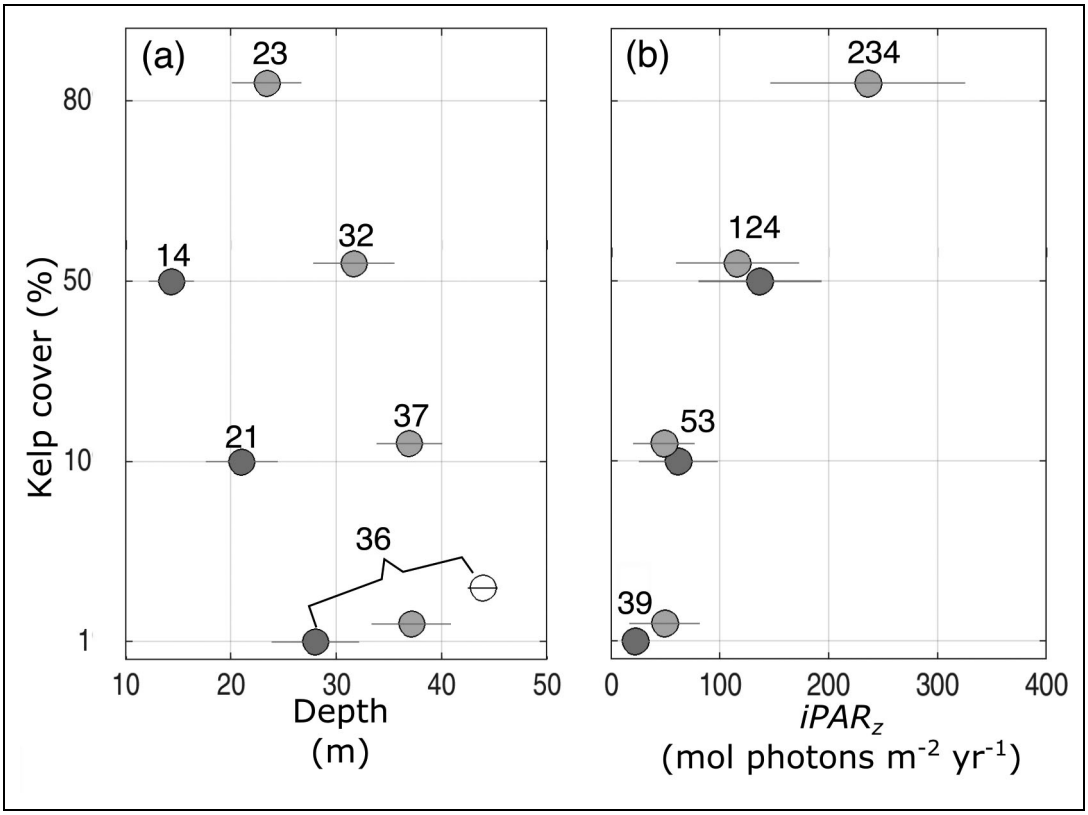

Figure 6. Relationships between the depth extent and underwater light environment of Arctic kelp forests. (a) Average maximum depth extent of the four target percentage kelp covers and (b) underwater light environment at this depth for kelp forests around Southampton Island (light grey), along western Greenland (dark grey) and offshore Disko Bay (white). Significant differences between regions were found for the depth of the 10 and 50% kelp cover. Numbers beside the symbols are the combined mean or the region-specific mean value for depth extent where significantly different. The 80% kelp cover data were only available for Southampton Island. Disko Bay data were only available for the depth extent of the 1% kelp cover, but κ_{dPAR} was not available to estimate $iPAR_z$. Note that the y-axis is non-linear.

observed to cover the nearshore environment of Hudson Bay, including around polynyas (Gupta et al., 2022). Therefore, landfast ice could have probably influenced OWL locally in the nearshore environment but was not resolved with our methods. The high-canopy kelps formed a higher percentage kelp cover and were more frequently found in shallow waters relative to areas where the low-canopy kelp species dominated. Although we did not regularly survey waters shallower than 5 m, occasional drop camera images between 1.5 and 3 m suggest that the rockweed *Fucus* sp. was the dominant macroalgal taxon in the lower littoral zone, with very little kelp observed.

The substratum type did not limit the kelp cover around SI, but it did influence the canopy height, with mixed substratum hosting more low-canopy kelp. The lack of relation between kelp cover and substratum mirrors findings in other parts of the Canadian Arctic for species like *Saccharina latissima*, *Alaria esculenta*, and *Laminaria solidungula* (Filbee-Dexter et al., 2022). Scuba diving confirmed that these species did not require extensive hard substrata to form high percentage kelp cover or biomass, with gravel or scattered cobbles on sediment being sufficient for kelps to attach. Similarly, there are observations in Kongsfjorden, Svalbard, of kelp growing on primarily sandy substratum (Hop et al., 2016). Around SI, rocky substrata were the most abundant substratum type, including in shallower waters, which contrasts with observations elsewhere in the western Arctic where sandy substrata can dominate shallow coastal regions (Dunton et al., 1982; Filbee-Dexter et al., 2022). The high abundance of rocky substrata around SI could be due to the prevailing intermediate-to-fast ocean currents (Video S1; Saucier et al., 2004), which are known to erode smaller-sized sediments (e.g., Pisareva et al., 2015). This high abundance of rocks and pebbles could be the reason for the absence of a relationship between substratum type and kelp cover around SI. Our results cannot confirm or refute previous findings of substratum limitation on the early stages of kelp, considering that sandy and mixed substrata are less ideal for gametophyte development and known to slow kelp recruitment and colonization (Spurkland and Iken, 2011a; Konar, 2013; Desmond et al., 2015; Traiger and Konar, 2017; Huovinen et al., 2020; Bonsell and Dunton, 2021).

The OWL was the best predictor of the kelp depth extent around SI, supporting previous findings of the dominant role of sea-ice-mediated light-limited environment in

Table 2. Minimum light required by Arctic kelp as reported by different sources

Region	[a]$iPAR_z$	Depth (m)	Water Clarity	[b]Source
Southampton Island	49	37	Highly clear	This study
Foxe Basin	49	20	Highly clear	Chapman and Lindley (1980)
Beaufort Sea Lagoons	45–50	5	Highly turbid	Dunton (1990)
Hansneset, Kongsfjorden	42	15	Highly turbid	Bartsch et al. (2016)
Young Sound	40	15–20	Turbid	Borum et al. (2002)

[a]$iPAR_z$ depends on $iPAR^{0+}$, depth, water clarity, and open water days with light (OWL); units for $iPAR_z$ are mol photons m^2 yr^{-1}.

[b]Small differences between estimates are expected due to our need to maintain κ_{dPAR} constant throughout the year, and use parametrizations to account for the loss of light at the air-ocean interface due to the high solar zenith angle in polar regions (as described in the Methods).

determining Arctic kelp depth extent in Greenland (Krause-Jensen et al., 2012) and kelp spatial distribution throughout the Eastern Canadian Arctic (Goldsmit et al., 2021; Filbee-Dexter et al., 2022). The relationship between kelp depth extent versus OWL was stronger when combining datasets from SI, western Greenland and Disko Bay. The combined data also highlighted that the more southerly kelp observations along western Greenland (stations Nuuk-1 and Itelleq), with the longest OWL but relatively shallow kelp depth extent, could be outliers to this relationship. Such outliers could relate to species-specific adaptations to deeper waters; for instance, these two stations were the only ones in the dataset without *Saccharina latissima* (Krause-Jensen et al., 2012).

The lack of relationship between kelp depth extent and water temperature (at the depth extent) could be influenced by the small variability in temperature between stations and the relatively cold environment (from -0.6 to 4°C). This result agrees with recent observations in the Eastern Canadian Arctic that suggest that kelp distribution is driven by sea ice rather than temperature (Filbee-Dexter et al., 2022). We note that, while experimental and field studies have linked warmer waters with enhanced kelp physiology (e.g., Fredersdorf et al., 2009; Iñiguez et al., 2016; Zacher et al., 2019; Li et al., 2020) and deeper kelp depth extent (Krause-Jensen et al., 2012), these studies have considered warmer waters and larger temperature ranges with maximum temperature exceeding 5°C, the upper temperature margin for suboptimal kelp growth (Wernberg et al., 2019). Ocean temperature may become more important in the regional kelp depth distribution in the future, with predicted ocean warming of 1 to 3°C in spring and summer in Hudson Bay (Joly et al., 2011; Bello and Higuchi, 2019). Some kelp species, like *Saccharina latissima*, to which SI is the northern limit of the species' range, may respond positively to regional increases in ocean temperature (Joly et al., 2011; Bello and Higuchi, 2019; Diehl et al., 2021), but obligated Arctic species like *Laminaria solidungula* may suffer disproportionate negative impacts even with moderate increases in temperature, as SI is on the southern limit of this species' range (Goldsmit et al., 2021).

Kelps are an essential energy input into the coastal marine food web (Duggins et al., 1989; Krumhansl and Scheibling, 2012). The simple, but significant, linear relationship between depth extent and OWL is key to mapping kelp cover and improving estimates of regional kelp net primary production. The potential area with at least 1% kelp covered around SI (approximately 27,000–28,000 km^2) along with local measurements of net primary production by *Saccharina latissima* and *Laminaria solidungula* at 15 m, 23.1–67.8 g C m^{-2} yr^{-1} (table S4 in Filbee-Dexter et al., 2022), results in a regional estimate of kelp net primary production between 0.6 and 1.9 TgC yr^{-1}. If considering the potential area with at least 50% kelp covered around SI (approximately 19,000–25,000 km^2) the net primary production estimate would be between 0.4 and 1.7 TgC yr^{-1}. These estimates should be seen as maxima, as they assumed that kelp production applied through the full depth range.

Another important variable for mapping the potential kelp depth distribution is the minimum underwater light required by kelp (Graham et al., 2007). Our estimate of 49 ± 32 mol photons m^2 yr^{-1} at the maximum depth extent (all-station median maximum of 37 m) is similar to previous measurements in the Arctic and Subarctic (**Table 2**; Chapman and Lindley, 1980; Dunton, 1990; Borum et al., 2002; Bartsch et al., 2016). As an example of the applications, the total standing stock of kelp in the Eastern Canadian Arctic was estimated at 72.7 ± 12.3 Tg C, assuming a maximum kelp depth extent of 30 m (Filbee-Dexter et al., 2022). However, if we consider that the maximum depth extent is closer to 40 m, as found around SI, the kelp standing stock would increase to 94.9 ± 16 Tg C under the premise of suitable substratum present (table S4 in Filbee-Dexter et al., 2022). To improve the minimum underwater light estimation, a consideration of seasonal variations in water transparency is important (e.g., κ_{dPAR}; Dunton, 1990). In a warmer future with less sea ice and more melting glaciers, the seasonal changes in water transparency may become even more relevant (Murray et al., 2015; Bonsell and Dunton, 2018; Huss and Hock, 2018), especially in coastal regions with active coastal erosion and large freshwater runoff from glaciers and rivers (e.g., Spurkland and Iken, 2011a; Murray et al., 2015; Hop

et al., 2016; Traiger and Konar, 2017; Bonsell and Dunton, 2018; Huovinen et al., 2020; Bonsell and Dunton, 2021).

Although water transparency was not a significant predictor of depth extent around SI, it was relevant in explaining the observed cross-regional differences in depth extent. Clearer waters around SI (κ_{dPAR} approximately 0.13 m^{-1}) at the end of the summer relative to western Greenland (κ_{dPAR} approximately 0.18 m^{-1}) created more favourable underwater light conditions, leading to the 15-m deeper depth extent of the 10 and 15% kelp cover around SI relative to western Greenland (**Figure 6a**), despite both regions having similar OWL and annual integrated incident irradiances. Indeed, clear water is a common characteristic of sites reporting deep kelp, from equatorial (Spalding et al., 2003; Graham et al., 2007) to polar regions, despite the shorter light period at high latitudes (Chapman and Lindley, 1980). Higher water transparency can also explain the deeper, and more productive, kelp ecosystems at offshore relative to nearshore sites in Arctic Alaska (Aumack et al., 2007), Greenland (Krause-Jensen et al., 2019) and Svalbard (Hop et al., 2016). Contrastingly, poor water transparency is associated with shallower kelp depth extent and reduced kelp abundance (Desmond et al., 2015; Huovinen et al., 2020). Comparisons of the water transparency index κ_{dPAR}, must, however, be interpreted with caution, as the magnitude of κ_{dPAR} depends strongly on the thickness and position of the depth layer considered in the calculations. κ_{dPAR} values tend to decrease with depth as blue and red wavelengths are quickly absorbed in the top layer (Morel et al., 2007). Hence, the use of a consistent depth interval is recommended for comparison among regions but is difficult to accomplish.

The recent (2014–2020) rapid losses of Arctic sea ice, for example, has increased the OWL and annual integrated PAR reaching the ocean surface (Gattuso et al., 2020; Singh et al., 2022), but climate warming combined with the longer ice-free season has also acted to increase coastal erosion, runoff, and frequency of sediment resuspension from storm events (Bonsell and Dunton, 2018), resulting in increased turbidity and the halt in the upward trend of averaged underwater PAR (Singh et al., 2022). Increasing turbidity could result in a shallowing of the kelp depth extent due to less light reaching the benthos, or a shift of kelp towards deeper, but clearer, waters offshore (Aumack et al., 2007; Traiger and Konar, 2017; Krause-Jensen et al., 2019). Other environmental conditions may also be driving a kelp depth redistribution. For instance, decreasing salinity close to the coast due to increasing river runoff can affect the physiology of some kelp species negatively (Spurkland and Iken, 2011b; Lind and Konar, 2017; Li et al., 2020). Likewise, silt and sediment in the water column can have negative effects on the physiology of kelp when sediments deposit on kelp fronds (Roleda and Dethleff, 2011; Huovinen et al., 2020) or when it accumulates on the substratum forming a thick sandy/silty layer unsuitable for kelp attachment and recruitment (Spurkland and Iken, 2011a; Desmond et al., 2015; Hop et al., 2016; Zacher et al., 2016; Lind and Konar, 2017; Traiger and Konar, 2017; Huovinen et al., 2020). Conversely, sediment deposition on kelp blades might be beneficial by mitigating harmful ultraviolet radiation effects (Roleda et al., 2008; Roleda and Dethleff, 2011).

Intense phytoplankton blooms may also affect the underwater light environment, and thus the depth extent of kelp. This effect would be especially true around SI, where there are no glaciers or large river runoff. Spring and summer phytoplankton blooms are particularly intense in the northwest polynya of Hudson Bay near the southwest coast of SI (Barbedo et al., 2020). Phytoplankton blooms can shade the benthos by capturing the photosynthetically usable radiation (PUR; sensu Morel, 1978; Bélanger et al., 2013). Phytoplankton shading of kelp forest has been documented in tropical upwelling regions (Graham et al., 2007) and along Greenland fjords (Murray et al., 2015). Phytoplankton may also be in a competitive relationship with kelp for nutrients as revealed by observation of low phytoplankton productivity above a dense kelp system in shallow waters in western Hudson Bay (Keats et al., 1989) and within the Strait of Juan de Fuca in the Pacific Ocean (Pfister et al., 2019). Although, nutrient concentration may have a secondary role in the growth of Arctic kelp relative to underwater light (Chapman and Lindley, 1980; Henley and Dunton, 1997), it can still influence kelp distribution (e.g., Chapman and Lindley, 1980; Steneck et al., 2012; Franco et al., 2018; Filbee-Dexter et al., 2019), especially when considering the generally low concentration of nutrients throughout the Eastern Canadian Arctic (Filbee-Dexter et al., 2019).

We did not consider spatial patterns in ocean currents as a driver of kelp depth extent; however, water motion has been suggested to impact kelp growth regardless of the underwater light environment or nutrient concentrations (Hurd, 2000; Hepburn et al., 2007; Kregting et al., 2016). Kelp growth rates are lower in areas with ocean currents that are either slow (<0.1–0.2 m s^{-1}) or especially fast (>12–1.5 m s^{-1}) relative to areas with intermediate currents (>0.1 m s^{-1} and <1.2 m s^{-1}) (Kraemer and Chapman, 1991; Hurd, 2000; Kregting et al., 2015, 2016). Model simulations (Saucier et al., 2004), Traditional Knowledge (Westdal et al., 2010) and our observations during sampling suggest that SI has a diverse hydrodynamic environment: intermediate ocean currents (0.4–0.8 m s^{-1}) in the west, within Roes Welcome Sound, and along the southwest coast (Saucier et al., 2004), and fast ocean currents (1.4 m s^{-1}) in the northern parts of Roes Welcome Sound and along the northeast coast (Saucier et al., 2004; Westdal et al., 2010). We estimated ocean currents with intermediate speed on the southern part of Roes Welcome Sound (0.8 m s^{-1}, from vessel drift speed), and observed apparently fast currents in a video recording taken at 46 m on August 13, 2019 near Station 12.2 on the northern parts of Roes Welcome Sound (Video S1; Figure S4). This video shows structural damage to kelp blades, which is a common consequence in fast-flow environments (Gerard and Mann, 1979; Kraemer and Chapman, 1991; Kregting et al., 2016). A more detailed assessment of the hydrodynamic and nutrient environment around SI could further explain patterns in kelp depth extent, especially in

light of a recent modelling study that predicts a decrease in kelp cover in response to future changes in ocean dynamics around SI (Goldsmit et al., 2021).

This study found that SI coastal region is characterized by cold waters, high water transparency (e.g., low κ_{dPAR}), large OWL, low grazing pressure, abundant suitable substrata, and deep and extensive kelp forests. OWL was the principal explanatory variable of kelp depth extent from a suit of five variables. This relationship was used to make the first estimates of maximum present-day extent of kelp around this Island. We combined the summer κ_{dPAR} and the length of OWL to determine the minimal light required by kelp, another important tool for mapping the area covered by kelp forests. Understanding the drivers of Arctic kelp depth extent will help improve estimates of current and future distribution of kelp, which has implications for better understanding Arctic coastal ecology and the role of kelp forests.

Data accessibility statement

The following data sets were used in this study:

- In situ data used in the analysis presented are included in the supporting materials Tables S1–S2.
- CTD and rosette profiles taken around Southampton Island in 2018 and 2019 are available at https://doi.org/10.34992/dc0p-kf56.
- Temperature climatology were downloaded from HTTPServer: /thredds-ocean/fileServer/ncei/woa/temperature/decav/0.25/woa18_decav_t08_04.nc.
- Salinity climatology were downloaded from HTTPServer: /thredds-ocean/fileServer/ncei/woa/salinity/decav/0.25/woa18_decav_s08_04.nc.
- Sea ice concentration from AMSRE were downloaded from https://seaice.uni-bremen.de/data/amsr2/asi_daygrid_swath/n6250/.
- Sea ice concentration from PMW-bootstrapV3 algorithm were downloaded from https://doi.org/10.5067/7Q8HCCWS4I0R.
- Downward shortwave radiation data used to calculate PAR^{0+} were downloaded from https://open.canada.ca/data/en/dataset/c041e79a-914a-5a4e-a485-9cbc506195df.
- Bathymetry data were from ETOPO1 global relief model doi:10.7289/V5C8276M.

Supplemental files

The supplemental files for this article can be found as follows:

- **Table S1.** Environmental conditions observed around Southampton Island.
- **Table S2.** Environmental characteristics at the depth extent of kelp at stations around Southampton Island.
- **Table S3.** Greenland data on kelp depth extent and environmental conditions.
- **Table S4.** Spearman Rank Correlation matrix for variables consider in the depth extent analysis.
- **Figure S1.** Example classifications of kelp cover, canopy and substratum type.
- **Figure S2.** Relationship between percent kelp cover and depth around Southampton Island.
- **Figure S3.** Kelp depth extent as a function of kelp assemblage and substratum type around Southampton Island.
- **Figure S4.** An angled kelp with torn blade growing in a fast current environment.
- **Video S1.** Fast currents vigorously angle a kelp blade at 46 m on August 13, 2019 near Station 12.2 on the northern parts of Roes Welcome Sound.

Acknowledgments

We thank the Aiviit and Aiviq Hunters and Trappers Organizations for their support of this research, the 2018 and 2019 crew and research staff R/V *William Kennedy*, and Prof. Paul G. Myers for providing access to Compute Canada Resources where all analyses were conducted. We would like to thank the reviewers for taking the necessary time and effort to review this manuscript.

Funding

This research was funded through: the Marine Environmental Observation, Prediction and Response Network of Centres of Excellence (MEOPAR-NCE), Polar Knowledge Canada, and National Science and Engineering Research Council of Canada (NSERC) ship time grants for the *Southampton Island Marine Ecosystem Project* (SIMEP, https://doi.org/10.34992/dc0p-kf56, to CJM); the 2017–2018 Belmont Forum and BiodivERsA joint call for research proposals under the BiodivScen ERA-Net COFUND programme to the project ACCES: *De-icing of Arctic coasts: Critical or new opportunities for marine biodiversity and ecosystem services?* with funding organizations National Science Foundation (NSF; project nr. 1906726 to KI and BK), Natural Science and Engineering Research Council of Canada (NSERC; project nr. RGPBB 523763-2018 to CJM and project nr. RGPIN-2019-06070 to SB), Fonds de recherche du Québec -Nature et technologies (FRQNT; project nr. 270860 to SB) and Research Council of Norway (RCN; project nr. 296836 to JES); NSERC Discovery Grant and Northern Research Supplements to SB, PA, CJM; ArcticNet (project nr. P101 ArcticKelp, htts://www.arctickelp.ca, to PA, KFD, and LEJ); NSERC Postdoctoral Fellowship program (NSERC-PDF; project nr. 516938-2018 to KFD) and Australian Research Council DECRA (project nr. DE1901006192 to KFD). Furthermore, this study was supported in part by the Churchill Marine Observatory (CMO), which was funded by the Canada Foundation for Innovation and other partners, including the Arctic Research Foundation (ARF). This work represents a contribution to the Canada Excellence Research Chair (CERC) unit at the University of Manitoba.

Competing interests

The authors have no competing interests, as defined by *Elementa*, that might be perceived to influence the research presented in this manuscript.

Author contributions

Contributed to conception and design: LCG, JR, KAM, BK, KI, CJM.

Contributed to acquisition of data: LCG, KFD, JR, KAM, IG, BK, KI, CJM.

Contributed to analysis and interpretation of data: All authors.

Drafted the first version of the manuscript: LCG, CJM.

Revised the article: All authors.

Approved the submitted version for publication: All authors.

References

Amante, C, **Eakins, BW.** 2009. ETOPO1 1 Arc-minute global relief model: Procedures, data sources and analysis. *NOAA Technical Memorandum NESDIS NGDC-24* **19**. DOI: http://dx.doi.org/10.7289/V5C8276M. Accessed March 2022.

Aumack, CF, **Dunton, KH**, **Burd, AB**, **Funk, DW**, **Maffione, RA.** 2007. Linking light attenuation and suspended sediment loading to benthic productivity within an Arctic kelp-bed community. *Journal of Phycology* **43**(5): 853–863. DOI: http://dx.doi.org/10.1111/j.1529-8817.2007.00383.x.

Barbedo, L, **Bélanger, S**, **Tremblay, JE.** 2020. Climate control of sea-ice edge phytoplankton blooms in the Hudson Bay system. *Elementa: Science of the Anthropocene* **8**(1). DOI: http://dx.doi.org/10.1525/elementa.039.

Bartsch, I, **Paar, M**, **Fredriksen, S**, **Schwanitz, M**, **Daniel, C**, **Hop, H**, **Wiencke, C.** 2016. Changes in kelp forest biomass and depth distribution in Kongsfjorden, Svalbard, between 1996–1998 and 2012–2014 reflect Arctic warming. *Polar Biology* **39**(11): 2021–2036. DOI: http://dx.doi.org/10.1007/s00300-015-1870-1.

Bélanger, S, **Babin, M**, **Tremblay, JE.** 2013. Increasing cloudiness in Arctic damps the increase in phytoplankton primary production due to sea ice receding. *Biogeosciences* **10**(6): 4087–4101. DOI: http://dx.doi.org/10.5194/bg-10-4087-2013.

Bello, R, **Higuchi, K.** 2019. Changing surface radiation and energy budgets of the Hudson Bay Complex using the North American regional reanalysis (NARR) model. *Arctic Science* **5**(4): 218–239. DOI: http://dx.doi.org/10.1139/as-2018-0034.

Bluhm, BA, **Brown, K**, **Rotermund, L**, **Williams, W**, **Danielsen, S**, **Carmack, EC.** 2022. New distribution records of kelp in the Kitikmeot Region, Northwest Passage, Canada, fill a pan-Arctic gap. *Polar Biology* **45**(4): 719–736. DOI: http://dx.doi.org/10.1007/s00300-022-03007-6.

Bonsell, C, **Dunton, KH.** 2018. Long-term patterns of benthic irradiance and kelp production in the central Beaufort sea reveal implications of warming for Arctic inner shelves. *Progress in Oceanography* **162**: 160–170. DOI: http://dx.doi.org/10.1016/j.pocean.2018.02.016.

Bonsell, C, **Dunton, KH.** 2021. Slow community development enhances abiotic limitation of benthic community structure in a high Arctic kelp bed. *Frontiers in Marine Science* **8**: 21. DOI: http://dx.doi.org/10.3389/fmars.2021.592295.

Borum, J, **Pedersen, M**, **Krause-Jensen, D**, **Christensen, P**, **Nielsen, K.** 2002. Biomass, photosynthesis and growth of *Laminaria saccharina* in a high-arctic fjord, NE Greenland. *Marine Biology* **141**(1): 11–19. DOI: http://dx.doi.org/10.1007/s00227-002-0806-9.

Chapman, ARO, **Lindley, JE.** 1980. Seasonal growth of *Laminaria solidungula* in the Canadian High Arctic in relation to irradiance and dissolved nutrient concentrations. *Marine Biology* **57**(1): 1–5. DOI: http://dx.doi.org/10.1007/BF00420961.

Comiso, JC. 2017. Bootstrap Sea Ice Concentrations from Nimbus-7 SMMR and DMSP SSM/ISSMIS, Version 3 [2007–2009]. Boulder, CO: NASA National Snow and Ice Data Center Distributed Active Archive Center. DOI: http://dx.doi.org/10.5067/7Q8HCCWS4I0R.

Dayton, PK. 1985. Ecology of kelp communities. *Annual Review of Ecology and Systematics* **16**: 215–245. http://www.jstor.org/stable/2097048.

Desmond, MJ, **Pritchard, DW**, **Hepburn, CD.** 2015. Light limitation within southern New Zealand kelp forest communities. *PLoS One* **10**(4): 1–18. DOI: http://dx.doi.org/10.1371/journal.pone.0123676.

Diehl, N, **Roleda, MY**, **Bartsch, I**, **Karsten, U**, **Bischof, K.** 2021. Summer heatwave impacts on the European kelp *Saccharina latissima* across its latitudinal distribution gradient. *Frontiers in Marine Science* **8**. DOI: http://dx.doi.org/10.3389/fmars.2021.695821.

Duggins, DO, **Simenstad, CA**, **Estes, JA.** 1989. Magnification of secondary production by kelp detritus in coastal marine ecosystems. *Science* **245**(4914): 170–173. DOI: http://dx.doi.org/10.1126/science.245.4914.170.

Dunton, K, **Jodwalis, C.** 1988. Photosynthetic performance of *Laminaria solidungula* measured in situ in the Alaskan High Arctic. *Marine Biology* **98**(2): 277–285. DOI: http://dx.doi.org/10.1007/BF00391206.

Dunton, KH. 1990. Growth and production in *Laminaria solidungula*: Relation to continuous underwater light levels in the Alaskan High Arctic. *Marine Biology* **106**(2): 297–304. DOI: http://dx.doi.org/10.1007/BF01314813.

Dunton, KH, **Reimnitz, E**, **Schonberg, S.** 1982. An Arctic kelp community in the Alaskan Beaufort Sea. *Arctic* **35**(4): 457–571. DOI: http://dx.doi.org/10.14430/arctic2355.

Dunton, KH, **Reimnitz, E**, **Schonberg, S.** 2013. The role of coastal plant communities for climate change mitigation and adaptation. *Nature Climate Change* **3**(11): 961–968. DOI: http://dx.doi.org/10.1038/nclimate1970.

Fieler, R, **Greenacre, M**, **Matsson, S**, **Neves, L**, **Forbord, S**, **Hancke, K.** 2021. Erosion dynamics of cultivated kelp, *Saccharina latissima*, and implications for environmental management and carbon sequestration.

Frontiers in Marine Science **8**. DOI: http://dx.doi.org/10.3389/fmars.2021.632725.

Filbee-Dexter, K, **MacGregor, KA**, **Lavoie, C**, **Garrido, I**, **Goldsmit, J**, **Castro de la Guardia, L**, **Howland, KL**, **Johnson, LE**, **Konar, B**, **McKindsey, CW**, **Mundy, CJ**, **Schlegel, RW**, **Archambault, P.** 2022. Sea ice and substratum shape extensive kelp forests in the Canadian Arctic. *Frontiers in Marine Science* **9**: 754074. DOI: http://dx.doi.org/10.3389/fmars.2022.754074.

Filbee-Dexter, K, **Scheibling, RE.** 2017. The present is the key to the past: Linking regime shifts in kelp beds to the distribution of deep-living sea urchins. *Ecology* **98**(1): 253–264. DOI: http://dx.doi.org/10.1002/ecy.1638.

Filbee-Dexter, K, **Wernberg, T**, **Fredriksen, S**, **Norderhaug, KM**, **Pedersen, MF.** 2019. Arctic kelp forests: Diversity, resilience and future. *Global and Planetary Change* **172**: 1–14. DOI: http://dx.doi.org/10.1016/j.gloplacha.2018.09.005.

Franco, JN, **Tuya, F**, **Bertocci, I**, **Rodríguez, L**, **Martínez, B**, **Sousa-Pinto, I**, **Arenas, F.** 2018. The 'golden kelp' *Laminaria ochroleuca* under global change: Integrating multiple eco-physiological responses with species distribution models. *Journal of Ecology* **106**(1): 47–58. DOI: http://dx.doi.org/10.1111/1365-2745.12810.

Fredersdorf, J, **Müller, R**, **Becker, S**, **Wiencke, C**, **Bischof, K.** 2009. Interactive effects of radiation, temperature and salinity on different life history stages of the Arctic kelp *Alaria esculenta* (Phaeophyceae). *Oecologia* **160**: 483–493. DOI: http://dx.doi.org/10.1007/s00442-009-1326-9.

Gattuso, JP, **Gentili, B**, **Antoine, D**, **Doxaran, D.** 2020. Global distribution of photosynthetically available radiation on the seafloor. *Earth System Science Data* **12**(3): 1697–1709. DOI: http://dx.doi.org/10.5194/essd-12-1697-2020.

Gattuso, JP, **Gentili, B**, **Duarte, CM**, **Kleypas, JA**, **Middelburg, JJ**, **Antoine, D.** 2006. Light availability in the coastal ocean: Impact on the distribution of benthic photosynthetic organisms and their contribution to primary production. *Biogeosciences* **3**(4): 489–513. DOI: http://dx.doi.org/10.5194/bg-3-489-2006.

Gerard, VA, **Mann, KH.** 1979. Growth and production of *Laminaria longicruris* (Phaeophyta) populations exposed to different intensities of water movement. *Journal of Phycology* **15**(1): 33–41. DOI: http://dx.doi.org/10.1111/j.1529-8817.1979.tb02958.x.

Goldsmit, J, **Schlegel, RW**, **Filbee-Dexter, K**, **MacGregor, KA**, **Johnson, LE**, **Mundy, CJ**, **Savoie, AM**, **McKindsey, CW**, **Howland, KL**, **Archambault, P.** 2021. Kelp in the Eastern Canadian Arctic: Current and future predictions of habitat suitability and cover. *Frontiers in Marine Science* **8**: 1453. DOI: http://dx.doi.org/10.3389/fmars.2021.742209.

Graham, MH, **Kinlan, BP**, **Druehl, LD**, **Garske, LE**, **Banks, S.** 2007. Deep-water kelp refugia as potential hotspots of tropical marine diversity and productivity. *Proceedings of the National Academy of Sciences* **104**(42): 16576–16580. DOI: http://dx.doi.org/10.1073/pnas.0704778104.

Gupta, K, **Mukhopadhyay, A**, **Babb, DG**, **Barber, DG**, **Ehn, JK.** 2022. Landfast sea ice in Hudson Bay and James Bay: Annual cycle, variability and trends, 2000–2019. *Elementa: Science of the Anthropocene* **10**(1). DOI: http://dx.doi.org/10.1525/elementa.2021.00073.

Henley, WJ, **Dunton, KH.** 1997. Effects of nitrogen supply and continuous darkness on growth and photosynthesis of the arctic kelp *Laminaria solidungula*. *Limnology and Oceanography* **42**(2): 209–216. DOI: http://dx.doi.org/10.4319/lo.1997.42.2.0209.

Hepburn, CD, **Holborow, JD**, **Wing, SR**, **Frew, RD**, **Hurd, CL.** 2007. Exposure to waves enhances the growth rate and nitrogen status of the giant kelp *Macrocystis pyrifera*. *Marine Ecology Progress Series* **339**: 99–108. DOI: http://dx.doi.org/10.3354/meps339099.

Hop, H, **Kovaltchouk, NA**, **Wiencke, C.** 2016. Distribution of macroalgae in Kongsfjorden, Svalbard. *Polar Biology* **39**(11): 2037–2051. DOI: http://dx.doi.org/10.1007/s00300-016-2048-1.

Huovinen, P, **Ramírez, J**, **Palacios, M**, **Gómez, I.** 2020. Satellite-derived mapping of kelp distribution and water optics in the glacier impacted Yendegaia Fjord (Beagle Channel, Southern Chilean Patagonia). *Science of The Total Environment* **703**: 135531. DOI: http://dx.doi.org/10.1016/j.scitotenv.2019.135531.

Hurd, CL. 2000. Water motion, marine macroalgal physiology, and production. *Journal of Phycology* **36**(3): 453–472. DOI: http://dx.doi.org/10.1046/j.1529-8817.2000.99139.x.

Huss, M, **Hock, R.** 2018. Global-scale hydrological response to future glacier mass loss. *Nature Climate Change* **8**(2): 135–140. DOI: http://dx.doi.org/10.1038/s41558-017-0049-x.

Iñiguez, C, **Carmona, R**, **Lorenzo, MR**, **Niell, FX**, **Wiencke, C**, **Gordillo, FJL.** 2016. Increased temperature, rather than elevated CO_2, modulates the carbon assimilation of the Arctic kelps *Saccharina latissima and Laminaria solidungula*. *Marine Biology* **163**(12): 248. DOI: http://dx.doi.org/10.1007/s00227-016-3024-6.

Joly, S, **Senneville, S**, **Caya, D**, **Saucier, FJ.** 2011. Sensitivity of Hudson Bay Sea ice and ocean climate to atmospheric temperature forcing. *Climate Dynamics* **36**(9): 1835–1849. DOI: http://dx.doi.org/10.1007/s00382-009-0731-4.

Keats, D, **Green, JM**, **Hooper, RG.** 1989. Arctic algal communities in the region of Nuvuk Island, Northeastern Hudson Bay, Canada. *Le Naturaliste Canadien* **116**: 53–59. https://www.researchgate.net/publication/262009903_Arctic_algal_communities_in_the_region_of_the_Nuvuk_Islands_Northeastern_Hudson_Bay_Canada.

Kern, S, **Lavergne, T**, **Notz, D**, **Pedersen, LT**, **Tonboe, RT**, **Saldo, R**, **Sørensen, AM.** 2019. Satellite passive microwave sea-ice concentration data set intercomparison: Closed ice and ship-based observations. *The*

Cryosphere **13**(12): 3261–3307. DOI: http://dx.doi.org/10.5194/tc-13-3261-2019.

King, RJ, **Schramm, W.** 1976. Photosynthetic rates of benthic marine algae in relation to light intensity and seasonal variations. *Marine Biology* **37**(3): 215–222. DOI: http://dx.doi.org/10.1007/BF00387606.

Konar, B. 2013. Lack of recovery from disturbance in high-arctic Boulder communities. *Polar Biology* **36**(8): 1205–1214. DOI: http://dx.doi.org/10.1007/s00300-013-1340-6.

Kraemer, GP, **Chapman, DJ.** 1991. Biomechanics and alginic acid composition during hydrodynamic adaptation by *Egregia menziesii* (Phaeophyta) juveniles. *Journal of Phycology* **27**(1): 47–53. DOI: http://dx.doi.org/10.1111/j.0022-3646.1991.00047.x.

Krause-Jensen, D, **Archambault, P**, **Assis, J**, **Bartsch, I**, **Bischof, K**, **Filbee-Dexter, K**, **Dunton, KH**, **Maximova, O**, **Ragnarsdóttir, SB**, **Sejr, MK**, **Simakova, U**, **Spiridonov, V**, **Wegeberg, S**, **Winding, MHS**, **Duarte, CM.** 2020. Imprint of climate change on Pan-Arctic marine vegetation. *Frontiers in Marine Science* **7**: 1129. DOI: http://dx.doi.org/10.3389/fmars.2020.617324.

Krause-Jensen, D, **Duarte, CM.** 2016. Substantial role of macroalgae in marine carbon sequestration. *Nature Geoscience* **9**(10): 737–742. DOI: http://dx.doi.org/10.1038/ngeo2790.

Krause-Jensen, D, **Marbà, N**, **Olesen, B**, **Sejr, MK**, **Christensen, PB**, **Rodrigues, J**, **Renaud, PE**, **Balsby, TJ**, **Rysgaard, S.** 2012. Seasonal sea ice cover as principal driver of spatial and temporal variation in depth extension and annual production of kelp in Greenland. *Global Change Biology* **18**(10): 2981–2994. DOI: http://dx.doi.org/10.1111/j.1365-2486.2012.02765.x.

Krause-Jensen, D, **Marbà, N**, **Sanz-Martin, M**, **Hendriks, IE**, **Thyrring, J**, **Carstensen, J**, **Sejr, MK**, **Duarte, CM.** 2016. Long photoperiods sustain high pH in Arctic kelp forests. *Science Advances* **2**(12): e1501938. DOI: http://dx.doi.org/10.1126/sciadv.1501938.

Krause-Jensen, D, **Sejr, MK**, **Bruhn, A**, **Rasmussen, MB**, **Christensen, PB**, **Hansen, JL**, **Duarte, CM**, **Bruntse, G**, **Wegeberg, S.** 2019. Deep penetration of kelps offshore along the west coast of Greenland. *Frontiers in Marine Science* **6**: 375. DOI: http://dx.doi.org/10.3389/fmars.2019.00375.

Kregting, L, **Blight, AJ**, **Elsässer, B**, **Savidge, G.** 2016. The influence of water motion on the growth rate of the kelp *Laminaria digitata*. *Journal of Experimental Marine Biology and Ecology* **478**: 86–95. DOI: http://dx.doi.org/10.1016/j.jembe.2016.02.006.

Kregting, LT, **Hepburn, CD**, **Savidge, G.** 2015. Seasonal differences in the effects of oscillatory and unidirectional flow on the growth and nitrate-uptake rates of juvenile *Laminaria digitata* (Phaeophyceae). *Journal of Phycology* **51**(6): 1116–1126. DOI: http://dx.doi.org/10.1111/jpy.12348.

Krumhansl, KA, **Scheibling, RE.** 2012. Production and fate of kelp detritus. *Marine Ecology Progress Series* **467**: 281–302. DOI: http://dx.doi.org/10.3354/meps09940.

Kvifte, G, **Hegg, K**, **Hansen, V.** 1983. Spectral distribution of solar radiation in the Nordic countries. *Journal of Climate and Applied Meteorology* **22**(1): 143–152. Available at http://www.jstor.org/stable/26180904.

Laliberté, J, **Bélanger, S**, **Babin, M.** 2021. Seasonal and interannual variations in the propagation of photosynthetically available radiation through the Arctic atmosphere. *Elementa: Science of the Anthropocene* **9**(1). DOI: http://dx.doi.org/10.1525/elementa.2020.00083.

Li, H, **Monteiro, C**, **Heinrich, S**, **Bartsch, I**, **Valentin, K**, **Harms, L**, **Glöckner, G**, **Corre, E**, **Bischof, K.** 2020. Responses of the kelp *Saccharina latissima* (Phaeophyceae) to the warming Arctic: From physiology to transcriptomics. *Physiologia Plantarum* **168**(1): 5–26. DOI: http://dx.doi.org/10.1111/ppl.13009.

Lind, AC, **Konar, B.** 2017. Effects of abiotic stressors on kelp early life-history stages. *Algae* **32**(3): 223–233. DOI: http://dx.doi.org/10.4490/algae.2017.32.8.7.

Ling, S, **Cornwall, C**, **Tilbrook, B**, **Hurd, C.** 2020. Remnant kelp bed refugia and future phase-shifts under ocean acidification. *PLoS One* **15**(10): e0239136. DOI: http://dx.doi.org/10.1371/journal.pone.0239136.

Locarnini, R, **Mishonov, A**, **Baranova, O**, **Boyer, T**, **Zweng, M**, **Garcia, HE**, **Seidov, D**, **Weathers, K**, **Paver, C**, **Smolyar, I.** 2018. *World Ocean Atlas 2018, Volume 1: Temperature* (Levitus, S ed., Mishonov, A Technical ed.). Boulder, CO: NOAA Atlas NESDIS 81 [August 2005–2017]. Available at https://www.ncei.noaa.gov/data/oceans/woa/WOA18/DOC/woa18_vol1.pdf.

Lund-Hansen, L, **Valeur, J**, **Pejrup, M**, **Jensen, A.** 1997. Sediment fluxes, re-suspension and accumulation rates at two wind-exposed coastal sites and in a Sheltered Bay. *Estuarine, Coastal and Shelf Science* **44**(5): 521–531. DOI: http://dx.doi.org/10.1006/ecss.1996.0163.

Luneva, MV, **Aksenov, Y**, **Harle, JD**, **Holt, JT.** 2015. The effects of tides on the water mass mixing and sea ice in the Arctic Ocean. *Journal of Geophysical Research: Oceans* **120**(10): 6669–6699. DOI: http://dx.doi.org/10.1002/2014JC010310.

Lüning, K. 1991. *Seaweeds: Their environment, biogeography, and ecophysiology*. New York, NY: John Wiley & Sons.

Mohr, JL, **Wilimovsky, NJ**, **Dawson, EY.** 1957. An Arctic Alaskan kelp bed. *Arctic* **10**(1): 45–52. DOI: http://dx.doi.org/10.14430/arctic3754.

Mora-Soto, A, **Capsey, A**, **Friedlander, AM**, **Palacios, M**, **Brewin, PE**, **Golding, N**, **Dayton, P**, **Van Tussenbroek, B**, **Montiel, A**, **Goodell, W**, **Velasco-Charpentier, C.** 2021. One of the least disturbed marine coastal ecosystems on Earth: Spatial and temporal persistence of Darwin's sub-Antarctic giant kelp

forests. *Journal of Biogeography* **48**(10): 2562–2577. DOI: http://dx.doi.org/10.1111/jbi.14221.

Morel, A. 1978. Available, usable, and stored radiant energy in relation to marine photosynthesis. *Deep Sea Research* **25**(8): 673–688. DOI: http://dx.doi.org/10.1016/0146-6291(78)90623-9.

Morel, A. 1991. Light and marine photosynthesis: A spectral model with geochemical and climatological implications. *Progress in Oceanography* **26**(3): 263–306. DOI: http://dx.doi.org/10.1016/0079-6611(91)90004-6.

Morel, A, **Huot, Y**, **Gentili, B**, **Werdell, PJ**, **Hooker, SB**, **Franz, BA.** 2007. Examining the consistency of products derived from various ocean color sensors in open ocean (Case 1) waters in the perspective of a multi-sensor approach. *Remote Sensing of Environment* **111**(1): 69–88. DOI: http://dx.doi.org/10.1016/j.rse.2007.03.012.

Mork, M. 1996. The effect of kelp in wave damping. *Sarsia* **80**(4): 323–327. DOI: http://dx.doi.org/10.1080/00364827.1996.10413607.

Morris, RL, **Graham, TDJ**, **Kelvin, J**, **Ghisalberti, M**, **Swearer, SE.** 2020. Kelp beds as coastal protection: Wave attenuation of *Ecklonia radiata* in a shallow coastal bay. *Annals of Botany* **125**: 235–246. DOI: http://dx.doi.org/10.1093/aob/mcz127; https://pubmed.ncbi.nlm.nih.gov/31424534.

Mundy, C. 2017. Southampton Island Marine Ecosystem Project (SIMEP); Canadian Watershed Information Network (CanWIN), V1. Winnipeg, Canada: University of Manitoba. DOI: http://dx.doi.org/10.34992/dc0p-kf56.

Murie, KA, **Bourdeau, PE.** 2020. Fragmented kelp forest canopies retain their ability to alter local seawater chemistry. *Scientific Reports* **10**(1): 11039. DOI: http://dx.doi.org/10.1038/s41598-020-68841-2.

Murray, C, **Markager, S**, **Stedmon, CA**, **Juul-Pedersen, T**, **Sejr, MK**, **Bruhn, A.** 2015. The influence of glacial melt water on bio-optical properties in two contrasting Greenlandic fjords. *Estuarine, Coastal and Shelf Science* **163**: 72–83. DOI: http://dx.doi.org/10.1016/j.ecss.2015.05.041.

NOAA. 2009. *ETOPO1 1 Arc-Minute Global Relief Model*. Stennis Space Center, MS: NOAA National Centers for Environmental Information.

Pfister, CA, **Altabet, MA**, **Weigel, BL.** 2019. Kelp beds and their local effects on seawater chemistry, productivity, and microbial communities. *Ecology* **100**(10): e02798. DOI: http://dx.doi.org/10.1002/ecy.2798.

Pisareva, MN, **Pickart, RS**, **Iken, K**, **Ershova, EA**, **Grebmeier, JM**, **Cooper, LW**, **Bluhm, BA**, **Nobre, C**, **Hopcroft, RR**, **Hu, H**, **Wang, J**, **Ashjian, CJ**, **Kosobokova, KN**, **Whitledg, TE.** 2015. The relationship between patterns of benthic fauna and zooplankton in the Chukchi Sea and physical forcing. *Oceanography* **28**(3): 68–83. DOI: http://dx.doi.org/10.5670/oceanog.2015.58.

Prinsenberg, S, **Freeman, N.** 1986. Chapter 11 Tidal heights and currents in Hudson Bay and James Bay, in Martini, I ed., *Canadian Inland Seas, Elsevier Oceanography Series*. Amsterdam, the Netherlands: Elsevier: 205–216. (Elsevier Oceanography Series; vol. 44). DOI: http://dx.doi.org/10.1016/S0422-9894(08)70904-8.

Roleda, MY, **Dethleff, D.** 2011. Storm-generated sediment deposition on rocky shores: Simulating burial effects on the physiology and morphology of *Saccharina latissima* sporophytes. *Marine Biology Research* **7**(3): 213–223. DOI: http://dx.doi.org/10.1080/17451000.2010.497189.

Roleda, MY, **Dethleff, D**, **Wiencke, C.** 2008. Transient sediment load on blades of Arctic *Saccharina latissima* can mitigate UV radiation effect on photosynthesis. *Polar Biology* **31**(6): 765–769. DOI: http://dx.doi.org/10.1007/s00300-008-0434-z.

Ryther, JH. 1956. Photosynthesis in the ocean as a function of light intensity. *Limnology and Oceanography* **1**(1): 61–70. DOI: http://dx.doi.org/10.4319/lo.1956.1.1.0061.

Sager, J, **McFarlane, C.** 1997. Radiation, in Tibbitts, TW ed., *Plant growth chamber handbook*. Ames, IA: Iowa State University. Available at https://www.controlledenvironments.org/growth-chamber-handbook/.

Saucier, FJ, **Senneville, S**, **Prinsenberg, S**, **Roy, F**, **Smith, G**, **Gachon, P**, **Caya, D**, **Laprise, R.** 2004. Modelling the sea ice-ocean seasonal cycle in Hudson Bay, Foxe Basin and Hudson Strait, Canada. *Climate Dynamics* **23**(3): 303–326. DOI: http://dx.doi.org/10.1007/s00382-004-0445-6.

Schindelin, J, **Arganda-Carreras, I**, **Frise, E**, **Kaynig, V**, **Longair, M**, **Pietzsch, T**, **Preibisch, S**, **Rueden, C**, **Saalfeld, S**, **Schmid, B**, **Tinevez, J-Y**, **White, DJ**, **Hartenstein, V**, **Eliceiri, K**, **Tomancak, P**, **Cardona, A.** 2012. Fiji: An open-source platform for biological-image analysis. *Nature Methods* **9**(7): 676–682. DOI: http://dx.doi.org/10.1038/nmeth.2019.

Sharp, G, **Allard, M**, **Lewis, A**, **Semple, R**, **Rochefort, G.** 2008. The potential for seaweed resource development in subarctic Canada; Nunavik, Ungava Bay. *Journal of Applied Phycology* **20**(5): 491–498. DOI: http://dx.doi.org/10.1007/s10811-008-9323-7.

Singh, RK, **Vader, A**, **Mundy, CJ**, **Søreide, JE**, **Iken, K**, **Dunton, KH**, **Castro de la Guardia, L**, **Sejr, MK**, **Bélanger, S.** 2022. Satellite-derived photosynthetically available radiation at the coastal Arctic seafloor. *Remote Sensing* **14**(20). DOI: http://dx.doi.org/10.3390/rs14205180.

Smale, D, **Burrows, M**, **Moore, P**, **O'Connor, N**, **Hawkins, S.** 2013. Threats and knowledge gaps for ecosystem services provided by kelp forests: A northeast Atlantic perspective. *Ecology and Evolution* **3**(11): 4016–4038. DOI: http://dx.doi.org/10.1002/ece3.774.

Smith, GC, **Roy, F**, **Mann, P**, **Dupont, F**, **Brasnett, B**, **Lemieux, J-F**, **Laroche, S**, **Bélair, S.** 2014. A new atmospheric dataset for forcing ice-ocean models: Evaluation of reforecasts using the Canadian global deterministic prediction system. *Quarterly Journal of*

the Royal Meteorological Society **140**(680): 881–894. DOI: http://dx.doi.org/10.1002/qj.2194.

Spalding, H, **Foster, MS**, **Heine, JN.** 2003. Composition, distribution, and abundance of deep-water (>30 m) macroalgae in central California. *Journal of Phycology* **39**(2): 273–284. DOI: http://dx.doi.org/10.1046/j.1529-8817.2003.02010.x.

Spreen, G, **Kaleschke, L**, **Heygster, G.** 2008. Sea ice remote sensing using AMSR-E 89-GHz channels. *Journal of Geophysical Research: Oceans* **113**(C2). DOI: http://dx.doi.org/10.1029/2005JC003384.

Spurkland, T, **Iken, K.** 2011a. Kelp bed dynamics in estuarine environments in subarctic Alaska. *Journal of Coastal Research* **27**(6A): 133–143. DOI: http://dx.doi.org/10.2112/JCOASTRES-D-10-00194.1.

Spurkland, T, **Iken, K.** 2011b. Salinity and irradiance effects on growth and maximum photosynthetic quantum yield in subarctic *Saccharina latissima* (Laminariales, Laminariaceae). *Botanica Marina* **54**(4): 355–365. DOI: http://dx.doi.org/10.1515/bot.2011.042.

Steneck, RS, **Graham, MH**, **Bourque, BJ**, **Corbett, D**, **Erlandson, JM**, **Estes, JA**, **Tegner, MJ.** 2012. Kelp forest ecosystems: Biodiversity, stability, resilience and future. *Environmental Conservation* **29**(4): 459. DOI: http://dx.doi.org/10.1017/S0376892902000322.

Teagle, H, **Hawkins, SJ**, **Moore, PJ**, **Smale, DA.** 2017. The role of kelp species as biogenic habitat formers in coastal marine ecosystems. *Journal of Experimental Marine Biology and Ecology* **492**: 81–98. DOI: http://dx.doi.org/10.1016/j.jembe.2017.01.017.

Tideschart. 2022. Coats-Island tide times. Available at https://www.tideschart.com/Canada/Nunavut/Coats-Island/. Accessed September 9, 2022.

Traiger, SB, **Konar, B.** 2017. Supply and survival: Glacial melt imposes limitations at the kelp microscopic life stage. *Botanica Marina* **60**(6): 603–617. DOI: http://dx.doi.org/10.1515/bot-2017-0039.

Tummers, B. 2006. DataThief III. Available at https://datathief.org/. Accessed October 2021.

Weiskerger, CJ, **Rowe, MD**, **Stow, CA**, **Stuart, D**, **Johengen, T.** 2018. Application of the Beer–Lambert model to attenuation of photosynthetically active radiation in a shallow, eutrophic lake. *Water Resources Research* **54**(11): 8952–8962. DOI: http://dx.doi.org/10.1029/2018WR023024.

Wernberg, T, **Krumhansl, K**, **Filbee-Dexter, K**, **Pedersen, M.** 2019. Status and trends for the world's kelp forests, in Sheppard, C ed., *World seas: An environmental evaluation. 2nd ed.* Cambridge, MA: Academic Press: 57–78.

Westdal, K, **Richard, P**, **Orr, J.** 2010. Migration route and seasonal home range of the Northern Hudson Bay Narwhal (*Monodon monoceros*), in Ferguson, S, Loseto, L, Mallory, M eds., *A little less Arctic*. Dordrecht, the Netherlands: Springer. DOI: https://dx.doi.org/10.1007/978-90-481-9121-5_4.

Wiencke, C, **Amsler, CD.** 2012. Seaweeds and their communities in polar regions, in Wiencke, C, Bischof, K eds., *Seaweed biology: Novel insights into ecophysiology, ecology and utilization*. Berlin, Heidelberg: Springer Berlin Heidelberg: 265–291. DOI: http://dx.doi.org/10.1007/978-3-642-28451-9_13.

Wiktor, JM, **Tatarek, A**, **Kruss, A**, **Singh, RK**, **Wiktor, JM**, **Søreide, JE.** 2022. Comparison of macroalgae meadows in warm Atlantic versus cold Arctic regimes in the high-Arctic Svalbard. *Frontiers in Marine Science* **9**. DOI: http://dx.doi.org/10.3389/fmars.2022.1021675.

Zacher, K, **Bernard, M**, **Bartsch, I**, **Wiencke, C.** 2016. Survival of early life history stages of Arctic kelps (Kongsfjorden, Svalbard) under multifactorial global change scenarios. *Polar Biology* **39**(11): 2009–2020. DOI: http://dx.doi.org/10.1007/s00300-016-1906-1.

Zacher, K, **Bernard, M**, **Daniel Moreno, A**, **Bartsch, I.** 2019. Temperature mediates the outcome of species interactions in early life-history stages of two sympatric kelp species. *Marine Biology* **166**(12): 161. DOI: http://dx.doi.org/10.1007/s00227-019-3600-7.

Zweng, M, **Reagan, J**, **Seidov, D**, **Boyer, T**, **Locarnini, R**, **Garcia, H**, **Mishonov, A**, **Baranova, OK**, **Paver, C**, **Smolyar, I.** 2018. *World Ocean Atlas 2018, Volume 2: Salinity* (Levitus, S ed., Mishonov, A Technical ed.). Boulder, CO: NOAA Atlas NESDIS 82 [August 2005–2017]. Available at https://www.ncei.noaa.gov/data/oceans/woa/WOA18/DOC/woa18_vol2.pdf.

How to cite this article: Castro de la Guardia, L, Filbee-Dexter, K, Reimer, J, MacGregor KA, Garrido, I, Singh RK, Bélanger, S, Konar, B, Iken K, Johnson, LE, Archambault, P, Sejr, MK, Søreide, JE, Mundy, CJ. 2023. Increasing depth distribution of Arctic kelp with increasing number of open water days with light. *Elementa: Science of the Anthropocene* 11(1). DOI: https://doi.org/10.1525/elementa.2022.00051

Domain Editor-in-Chief: Jody W. Deming, University of Washington, Seattle, WA, USA

Associate Editor: Laurenz Thomsen, Department of Marine Sciences, University of Gothenburg, Gothenburg, Sweden

Knowledge Domain: Ocean Science

Published: March 02, 2023 **Accepted:** January 31, 2023 **Submitted:** April 01, 2022

ELEMENTA Science of the Anthropocene

Elem Sci Anth is a peer-reviewed open access journal published by University of California Press.

OPEN ACCESS